An electrochemical system for efficiently harvesting low-grade heat energy

Citation: Lee, Seok Woo, Yuan Yang, Hyun-Wook Lee, Hadi Ghasemi, Daniel Kraemer, Gang Chen, and Yi Cui. "An Electrochemical System for Efficiently Harvesting Low-Grade Heat Energy." Nature Communications 5 (May 21, 2014).

As Published: http://dx.doi.org/10.1038/ncomms4942

Publisher: Nature Publishing Group

Persistent URL: http://hdl.handle.net/1721.1/92284

Version: Author's final manuscript: final author's manuscript post peer review, without publisher's formatting or copy editing

An electrochemical system for highly efficient harvesting of low-grade heat energy

Seok Woo Lee[1,a], Yuan Yang[2,a], Hyun-Wook Lee[1], Hadi Ghasemi[2], Daniel Kraemer[2], Gang Chen[2*], Yi Cui[1,3*]

[1]*Department of Materials Science and Engineering, Stanford University, Stanford, CA, 94305, USA.* [2]*Department of Mechanical Engineering, Massachusetts Institute of Technology, Cambridge, MA, 02139, USA.* [3]*Stanford Institute for Materials and Energy Sciences, SLAC National Accelerator Laboratory, 2575 Sand Hill Road, Menlo Park, CA 94025, USA.*

[a]These authors contributed equally to this work.

[*]To whom correspondence should be addressed. Email: gchen2@mit.edu and yicui@stanford.edu.

Abstract

Efficient and low-cost thermal energy harvesting systems are needed to utilize the tremendous low-grade heat sources. Although thermoelectric devices are attractive, its efficiency is limited by the relatively low figure-of-merit and low temperature differential. An alternative approach is to explore thermodynamic cycles. Thermogalvanic effect, the dependence of electrode potential on temperature, can construct such cycles. In one cycle, an electrochemical cell is charged at a temperature and then discharged at a different temperature with higher cell voltage, thereby converting heat to electricity. Here we report an electrochemical system using a copper hexacyanoferrate cathode and a Cu/Cu^{2+} anode

to convert heat into electricity. The electrode materials have low polarization, high charge capacity, moderate temperature coefficients and low specific heat. These features lead to a high heat-to-electricity energy conversion efficiency of 5.7 % when cycled between 10 and 60 ℃, opening a promising way to utilize low-grade heat.

Introduction

Low-grade heat sources (<100 °C) are ubiquitous, generated in energy conversion and utilization processes [1, 2]. Among the methods for converting this energy to electricity, thermoelectric (TE) materials and devices have been studied extensively for several decades [3-9]. Despite recent progress, however, the figure of merit (ZT) of thermoelectrics is limited to 2 at high temperatures and 1.5 below 100 °C [10, 11]. Seebeck effect in electrochemical system is also investigated for thermal energy harvesting in similar architectures as a thermoelectric device, but the efficiency achieved is usually lower than 0.5% below 100 °C since the thermopower is limited by poor ionic conductivity of electrolyte, which is more than three orders of magnitude smaller than electronic conductivity in state-of-the-art thermoelectric materials [12-15]. An alternative approach of electrochemical system for thermal energy harvesting is to explore thermodynamic cycle as in thermomechanical engines. Here we report an efficient thermally regenerative electrochemical cycle (TREC) based on the thermogalvanic effect, temperature dependence of electrode potential. For a half-cell reaction, $A + n\,e^- \rightarrow B$, the temperature coefficient is defined as

$$\alpha = \frac{\partial V}{\partial T} = \frac{\Delta S_{A,B}}{nF} \qquad \text{Eq. (1)}$$

where V is the electrode potential, T is temperature, n is the number of electrons transferred in the reaction, F is Faraday's constant, and $\Delta S_{A,B}$ is the partial molar entropy change for the half

cell reaction in isothermal condition (see Supplementary Note 1). This effect indicates that the voltage of a battery depends on temperature; thus a thermodynamic cycle can be constructed by discharging the battery at T_1 and charging back at T_2. If the charging voltage at T_2 is lower than the discharging voltage at T_1, net energy is produced by the voltage difference, originating from heat absorbed at the higher temperature, similar to a thermomechanical engine with the Carnot efficiency as the upper limit. In practice, instead of transport property limited in thermoelectric devices, the efficiency of TREC is limited by the heat capacity of materials and effectiveness of heat exchangers [16]. The concept of TREC was developed a few decades ago for high temperature applications (500 - 1500 ℃) and showed efficiency of 40-50% of the Carnot limit. But, low temperature TREC did not received as much attention since electrode materials with low polarization and high charge capacity at low temperature were limited [17]. Hammond et al. [18] tested an aqueous redox couple for low temperature solar-thermal applications, but the precipitation of reactants, large internal resistance, and poor solubility of active redox species causing large heat capacity of the system prevented them from reporting device operational characteristics and measuring the device efficiency, although a high efficiency was theoretically projected based on the measured open circuit voltage and 100% heat recuperation assumption. The recent development of highly reversible electrode materials with very low polarization loss during the research of rechargeable batteries has now made it possible for us to exploit the TREC concept in a new way.

In this report, we present a high-efficiency TREC for harvesting low-grade heat energy by employing solid copper hexacyanoferrate (CuHCF) as a positive electrode and Cu/Cu^{2+} as a negative electrode in an aqueous electrolyte. The fast kinetics, high charge capacity, high

temperature coefficient (α), and low heat capacity of these materials allow the system to operate with excellent efficiency.

Results

Working principle of TREC

To harvest thermal energy, the entire device undergoes a thermal cycle containing four processes: heating up, charging, cooling down, and discharging (Fig. 1a). This cycle is also plotted on a temperature-entropy (T-S) diagram to clarify the thermodynamics (Fig. 1b). In process 1, the cell is in the discharged state and heated from T_L to T_H (low to high temperature) at open circuit. Since CuHCF has a negative α and Cu/Cu^{2+} has a positive α, the open circuit voltage (OCV) of the full cell decreases during this process. The cell is then charged at a low voltage at T_H in process 2, and the entropy of the cell increases through heat absorption during the electrochemical reaction. In process 3, the cell is disconnected and cooled from T_H to T_L, and thus the OCV increases. In the final process, the cell is discharged at a higher voltage at T_L, and the entropy of the cell decreases through the ejection of heat into the environment. After the cycle, the system returns to the original discharged state at T_L. Since the charging voltage is lower than the discharging voltage, net work (W) is extracted as the difference between charging and discharging energy. This is the opposite of the consumption of energy due to electrochemical hysteresis during a typical charge/discharge cycle of a battery, since the charging energy here is partially provided by heat (Supplementary Fig. 1). Such a conversion process of thermal energy into electrochemical energy requires that the electrochemical voltage hysteresis during charge/discharge at a fixed temperature is much smaller than the voltage difference caused by temperature change, calling for the highly reversible electrochemical electrodes.

The efficiency of the system (η) is calculated as the net work (W) divided by the thermal energy input. If the enthalpy change ΔH and the entropy change ΔS are the same at T_H and T_L, which is a good approximation when $\Delta T = (T_H - T_L)$ is small, the maximum W is ΔTΔS (Fig. 1b). The energy input to complete the cycle includes two parts: the heat absorbed at T_H ($Q_H = T_H\Delta S$) and the external heat required to raise the temperature of the system (Q_{HX}). As part of heat rejected from the cooling process can be used for the heating process through heat recuperation, Q_{HX} can be expressed as $Q_{HX} = (1 - \eta_{HX})C_p\Delta T$, where C_p is the total heat capacity of the electrochemical cell, and η_{HX} is the efficiency of the heat recuperation (See Supplementary Fig. 2 and Supplementary Note 2). Consequently η can be expressed as:

$$h = \frac{W}{Q_H + Q_{HX}} = \frac{DTDS - E_{loss}}{T_H DS + (1 - h_{HX})C_p DT} \qquad \text{Eq. (2)}$$

where E_{loss} is the energy loss due to the cell electrical resistance. Note that $\Delta T\Delta S = \alpha Q_c \Delta T$, where Q_c is the charge capacity of the battery and α is the temperature coefficient of the electrochemical cell. The efficiency can be written as

$$h = h_c \frac{1 - I(R_H + R_L)/|a|DT}{1 + h_c(1 - h_{HX})/|Y|} \qquad \text{Eq. (3)}$$

where I is the current used in discharging and charging. R_H and R_L are the internal resistance at T_H and T_L, respectively. $Y = \alpha Q_c/C_p$, is a dimensionless parameter to describe the requirements of the system for high efficiency. A thorough derivation of efficiency is presented in Supplementary Note 3 and 4. If only the contributions of the electrode materials are considered, and it is assumed that both electrodes have the same properties except opposite signs of the temperature coefficient, $Y = \alpha q_c/c_p$ and it is defined as the figure of merit of an electrode material for TREC, but not thermocells. Here, q is the specific charge capacity and c_p is the specific heat

of an electrode. Consequently, it is clear that a higher temperature coefficient (α), a higher specific charge capacity (q_c), and a smaller specific heat (c_p) lead to higher efficiency for heat-to-electricity conversion. In addition, low voltage polarization and effective heat recuperation can also improve the efficiency. The value of Y for individual materials can be negative or positive, depending on the sign of the temperature coefficient, although efficiency expression takes its absolute value.

Electrochemical system for harvesting thermal energy

Considering these requirements, we have selected solid copper hexacyanoferrate (CuHCF) as the positive electrode for the TREC because of its negative temperature coefficient (-0.36 mV K^{-1}), high specific charge capacity (60 mAh g^{-1}) compared to redox couples in solution, relatively low specific heat (1.07 J $K^{-1}g^{-1}$), and ultra-low voltage hysteresis [19-21]. The corresponding figure of merit Y is as high as -0.073. For the negative electrode, a copper metal immersed in 3M $Cu(NO_3)_2$ aqueous solution is selected because of the high positive temperature coefficient (0.83 mV K^{-1}) of Cu/Cu^{2+} and its large specific charge capacity (825 mAh g^{-1} Cu). Although the corresponding Y for Cu alone is as high as 6.55, the electrolyte is an active component in the full cell and its contribution to heat capacity is considerable. Including the electrolytes, the corresponding Y are -0.031 and 0.125 for CuHCF/6M $NaNO_3$ and Cu/3M Cu^{2+}, respectively. Y for the full cell reaches -0.068 with both electrolyte and electrode considered (see Supplementary Table 1 and Supplementary Note 5). The relevant redox reactions at each electrode are $Na_{0.71}Cu[Fe^{III}(CN)_6]_{0.72} + a(Na^+ + e^-) = Na_{0.71+a}Cu[Fe^{III}(CN)_6]_{0.72-a}[Fe^{II}(CN)_6]_{0.72+a}$ and $Cu^{2+} + 2e^- = Cu$. The temperature coefficient of each electrode was tested by measuring the open-circuit voltage while varying temperature from 10 to 70 ℃. Figure 2a shows the OCV change of the

CuHCF electrode (50% state of charge), the Cu/Cu^{2+}(3M) electrode, and the full cell for each 10 ℃ increment when the voltage is set at 0 V at 10 ℃. The potentials of both electrodes exhibit a linear dependence on temperature, indicating a constant α in the temperature window tested. The measured temperature coefficients of CuHCF, Cu/Cu^{2+}, and the full cell are -0.36, 0.83, and -1.20 mV K^{-1}, respectively. These experimental values match with the expected ones. Figure 2b shows the voltage versus time plot of the full cell over one thermal cycle between 10 and 60 ℃ when the specific current density is 7.2 mA g^{-1} with respect to active materials (All current, energy, and power densities are based on the mass of active materials, including CuHCF, electrolyte for Na^{+}, copper, and water for Cu^{2+} in this paper.). In process 1, the OVC of the cell decreases from 0.406 to 0.337 V as the temperature increases from 10 to 60 ℃. Then the cell is charged for 250 min at 60 ℃ in process 2 and the voltage gradually increases. In process 3, the OCV of the cell increases from 0.613 to 0.679 V as the temperature decreases back to 10 ℃. The cell is discharged in process 4 at 10 ℃ until the voltage reaches the initial voltage of the discharged state at the beginning of process 1. The corresponding plot of voltage against specific charge capacity based on the mass of CuHCF is shown in Fig. 2c. The average charging voltage is 59.0 mV lower than the average discharging voltage and thus electrical energy is generated with a net energy density of 5.2 J g^{-1}. The voltage spikes at the beginning of each process are electrochemical in nature and are due to overpotential and internal resistance. At the end of process 4, the discharging curve forms nearly perfect closed loop with only tiny loss of electric charges. The Coulombic efficiency (ratio of the amount of charge extracted during discharging to that of adding in during charging) for this cycle is adequately high ~98.6 %.

Efficiency of TREC

The efficiency of the cycle is estimated based on equation 2. Effects of internal resistance and Coulombic efficiency are both taken into account. Details of calculations are shown in Supplementary Note 4 and Supplementary Fig. 3. Figure 3a plots the cycle efficiency versus the efficiency of heat recuperation when cycled between 10 and 60 ℃. The current density is 7.2 mA g^{-1}. When heat recuperation is not used, the cycle efficiency is 3.7%. The final system efficiency could be much higher when heat recuperation is used, depending on the efficiency of the heat recuperation system (η_{HX}). We have designed and tested two heat recuperation schemes using dummy cells and commercial battery cells, since the current laboratory cell is too small to match the heat exchanger size. The test combined with thermal modeling shows that heat recuperation efficiency (η_{HX}) between 45-80% can be achieved (details are shown in Supplementary Note 6.) In the following, we will assume 50% heat recuperation efficiency to discuss the cycle efficiency, which we believe is a conservative number. With 50% heat recuperation efficiency, the corresponding cycle efficiency increases to 5.7%. Figure 3b shows the efficiency at various cycling conditions with T_H varying between 40 and 70 ℃ and T_L fixed at 10 ℃. At a current density of 7.2 mA g^{-1} and η_{HX}=50%, the cycle efficiencies are 2.9 % for T_H=40 ℃, 4.8 % for 50 ℃, 5.7 % for 60 ℃, and 5.5 % for 70 ℃. The efficiency becomes higher as T_H increases because of larger voltage difference between the charging and discharging curves and faster kinetics at higher temperature. However, this tendency changes between a T_H of 60 and 70 ℃, since the Coulombic efficiency of CuHCF starts to decrease at these temperatures. When the temperature is higher than 80 ℃, significant decrease of Coulombic efficiency leads to rapid drop of the cycle efficiency (see Supplementary Fig. 4). When the current density increases to 17.9 mA g^{-1} for higher power output, the cycle efficiencies are still as high as 1.9 % for T_H=40 ℃, 3.2 % for 50 ℃, 5.0 % for 60 ℃, and 5.4 % for 70 ℃ despite the larger overpotential.

The efficiency is much higher than previous reports on thermogalvanic cells (Supplementary Table 2).

Long-term cycling

The cycling performance of the thermal energy harvesting system is shown in Fig. 4a. T_H and T_L are set to 50 and 20 ℃ to represent widely accessible temperatures of waste heat and room temperature, respectively. The current density is 17.9 mA g^{-1}. The energy density reaches 1.26 J g^{-1} in the initial cycle with an efficiency of 1.8%. The average efficiency is 1.7 % (η_{HX}=50%). Figure 4b compares the full cell voltage versus specific capacity of CuHCF for the 1st and 40th cycle. A slight shift of the loop is observed, but there is no significant change in the overall shape. In addition, the cycling performance of CuHCF at higher temperature is confirmed by long-term galvanostatic cycling of a CuHCF electrode at 70 ℃. At this temperature, the capacity decay is only 9.1% over 500 cycles (Supplementary Fig. 5). This result signifies that this TREC for thermal energy harvesting is expected to have stable cycling with further optimization.

Discussion

Since thermoelectric devices are major candidates for waste heat recovery, it is useful to point out the differences between thermoelectric devices and TREC. The ZT of thermoelectric materials are determined by transport properties, while the thermogalvanic figure of merit Y is determined by thermodynamic properties. Thermoelectric devices can have high power density, provided that one can manage heat flow on both hot and the cold sides to create the needed temperature difference, while TREC has relatively low power density. Its power density depends on applied current density and voltage gap between charging and discharging of a cycle. We

have estimated a power density of 1.2 mW g^{-1} for cell operating between 10 to 80 ℃ at current density of 58.5 mA g^{-1} with a one hour cycling time, based on the mass of all active materials and electrolytes (see Supplementary Fig. 6). Further improvement in power density can be realized by optimizing device configuration, utilizing porous copper electrode, and exploring new system with fast kinetics and large temperature coefficient (see Supplementary Note 7). On the other hand, due to its constant temperature operation, thermal management challenges, which are crucial for low-grade waste heat utilization, can be easier, as we have demonstrated in the heat recuperation testing (Supplementary Fig. 7-13 and Supplementary Table 3). With such an understanding first, we can now convert the efficiency achieved in TREC into familiar ZT in thermoelectric materials. The estimated ZT is 3.5 for the efficiency of 5.7 % when temperature is varied from 10 to 60 ℃, current density is 7.2 mA g^{-1}, and η_{HX}=50 % is considered in the calculation. When the current density increases to 17.9 mA g^{-1} (close to current density for maximum power density), the efficiency is 5.0 % and the estimated ZT is 2.7.

In this study, a thermally regenerative electrochemical system with CuHCF and Cu/Cu^{2+} electrodes is developed for low-grade thermal energy harvesting. The electrode materials have large temperature coefficients, high charge capacity, low specific heat, and small hysteresis. These properties lead to a high thermogalvanic figure of merit (Y) for the electrode materials and thus excellent heat-to-electricity conversion efficiency: a cycle efficiency of 3.7% between 10 ℃ and 60 ℃ without any heat recuperation and 5.7 % when 50% heat recuperation is assumed. The achieved cycle efficiency still has room to improve by improving heat recuperation efficiency and reducing the amount of electrolyte through increasing the concentration of salts [22, 23]. Furthermore, the efficiency improvement in this system is possible by searching for materials

with higher figure of merit and smaller hysteresis, especially solid electrode materials with a positive temperature coefficient as a counter electrode to CuHCF. In addition, further optimization is needed to improve the power output while maintaining high efficiency of thermal energy harvesting. Our work points to the great potential of TREC for utilizing ubiquitous low temperature heat sources.

Methods

Material synthesis and electrode preparation

Copper hexacyanoferrate (CuHCF) was synthesized by use of a simple co-precipitation method. 40 mM of $Cu(NO_3)_2$ and 20 mM of $K_3Fe(CN)_6$ (Sigma Aldrich) were prepared in 120 mL of distilled water, then both solutions were simultaneously added in drops into 60 mL of DI-water under vigorous stirring. A yellowish green precipitate formed during the precipitation. Then, the solid precipitate was filtered and washed several times with DI-water. Afterward, the precipitate was dried in vacuum oven at 40 °C for 12 h. The diameter of as-formed particles is typically below 100 nm (Supplementary Fig. 14) To prepare electrodes, a mixture of 70% wt/wt CuHCF, 20% wt/wt amorphous carbon (Timcal Super P Li), and 10% wt/wt polyvinylidene fluoride (Kynar HSV 900) was grounded by hand. 1-methyl-2-pyrrolidinone was added in the mixture to form slurry, which was spread on carbon cloth current collector (Fuel Cell Earth). The mass loading of CuCHF was between 2 and 3 mg on area of about 0.25 cm^2.

Electrochemical Characterizations

TREC is demonstrated as form of a flooded beaker cell as shown in Supplementary Fig. 3B. CuHCF on carbon cloth (~0.25 cm^2) is connected to working electrode. Cu foil (~4 cm^2) is connected to counter electrode. 6M $NaNO_3$ and 3M $Cu(NO_3)_2$ electrolytes are used for CuHCF and Cu electrodes, respectively. These electrolytes are separated by three anion exchange membranes (Selemion DSV, AGC engineering Co., LTD, Japan). Ag/AgCl in saturated KCl solution is located between the membranes as a reference

electrode. Electrochemical test of the cell is performed by a potentiostat with 50μV resolution (VM3, BioLogic). During the measurement, recording voltage was fluctuating ±0.2 mV due to noise. The temperature measurement uncertainty is estimated to be ±0.2℃ as we wait until equilibrium in an environment chamber (BTU-133, ESPEC North America, INC.) while the precision of the thermometer is ±0.1°C." The overall relative uncertainty in efficiency is estimated to be less than 3%, which corresponds to less than 0.2% in the absolute conversion efficiency.

Specific Heat Measurement

The specific heat (c_p) of the CuHCF was measured by Differential Scanning Calorimetry (DSC) test after drying the sample at 40~50 ℃ for more than 24 hours. The measurements were carried out by DSC Q100 (TA instrument). The measurement range was 20-70 ℃ with the ramping rate of 5 ℃/min. The heat flow curve is shown in Supplementary Fig. 15. The calculated c_p of CuHCF is 1.07 J $g^{-1}K^{-1}$.

Efficiency Calculation

The thermal-to-electricity efficiency is based on experimental charge/discharge curves of TREC cells. The specific heat is calculated based on experimental measurements. More details can be found in Supplementary Note 3 and 4.

References

1. Chu, S. & Majumdar, A. Opportunities and challenges for a sustainable energy future. *Nature* **488**, 294-303 (2012).
2. Rattner, A.S. & Garimella, S. Energy harvesting, reuse and upgrade to reduce primary energy usage in the USA. *Energy* **36**, 6172-6183 (2011).
3. Rosi, F.D. Thermoelectricity and thermoelectric power generation. *Solid-State Electronics* **11**, 833-868 (1968).
4. DiSalvo, F.J. Thermoelectric cooling and power generation. *Science* **285**, 703-706 (1999).
5. Bell, L.E. Cooling, heating, generating power, and recovering waste heat with thermoelectric systems. *Science* **321**, 1457-1461 (2008).

6. Poudel, B. et al. High-thermoelectric performance of nanostructured bismuth antimony telluride bulk alloys. *Science* **320**, 634-638 (2008).
7. Paradiso, J.A. & Starner, T. Energy Scavenging for Mobile and Wireless Electronics. *IEEE Pervasive Computing* **4**, 18-27 (2005).
8. Kraemer, D. et al. High-performance flat-panel solar thermoelectric generators with high thermal concentration. *Nature materials* **10**, 532-538 (2011).
9. Snyder, G.J. & Toberer, E.S. Complex thermoelectric materials. *Nature materials* **7**, 105-114 (2008).
10. Zebarjadi, M., Esfarjani, K., Dresselhaus, M.S., Ren, Z.F. & Chen, G. Perspectives on thermoelectrics: from fundamentals to device applications. *Energy & Environmental Science* **5**, 5147-5162 (2012).
11. Zhao, L.D. et al. Ultralow thermal conductivity and high thermoelectric figure of merit in SnSe crystals. *Nature* **508**, 373-377 (2014).
12. Kuzminskii, Y.V., Zasukha, V.A. & Kuzminskaya, G.Y. Thermoelectric effects in electrochemical systems. Nonconventional thermogalvanic cells *Journal of Power Sources* **52**, 231-242 (1994).
13. Quickenden, T.I. & Mua, Y. A review of power generation in aqueous thermogalvanic cells. *Journal of The Electrochemical Society* **142**, 3985-3994 (1995).
14. Hu, R. et al. Harvesting waste thermal energy using a carbon-nanotube-based thermo-electrochemical cell. *Nano letters* **10**, 838-846 (2010).
15. Gunawan, A. et al. Liquid Thermoelectrics: Review of Recent And Limited New Data of Thermogalvanic Cell Experiments. *Nanoscale and Microscale Thermophysical Engineering* **17**, 304-323 (2013).
16. Hesson, J.C. & Shimotake, H. in Regenerative EMF Cells, Vol. 64. (eds. C.E. Crouthamel & H.L. Recht) 82-104 (American Chemical Society, Washington, D.C.; 1967).
17. Chum, H.L. & Osteryoung, R.A. Review on thermally regenerative electrochemical system. (1981).
18. Hammond, R.H. & William M. Risen, J. An electrochemical heat engine for direct solar energy conversion. *Solar Energy* **23**, 443-449 (1979).
19. Wessells, C.D., Huggins, R.A. & Cui, Y. Copper hexacyanoferrate battery electrodes with long cycle life and high power. *Nature communications* **2**, 550-554 (2011).
20. Pasta, M., Wessells, C.D., Huggins, R.A. & Cui, Y. A high-rate and long cycle life aqueous electrolyte battery for grid-scale energy storage. *Nature communications* **3**, 1149-1155 (2012).
21. Wessells, C.D., Peddada, S.V., McDowell, M.T., Huggins, R.A. & Cui, Y. The effect of insertion species on nanostructured open framework hexacyanoferrate battery electrodes. *Journal of The Electrochemical Society* **159**, A98-A103 (2012).
22. Bejan, A. & Kraus, A.D. Heat Transfer Handbook. (Wiley-Interscience, 2003).
23. Serth, R.W. Process heat transfer: Principles and applications. (Academic Press, New York; 2007).

Acknowledgment

Y.C. acknowledges the support by the U.S. Department of Energy, Office of Basic Energy Sciences, Division of Materials Sciences and Engineering under Contract No. DE-AC02-76SF00515 through the SLAC National Accelerator Laboratory LDRD project. H.W.L acknowledges the support from Basic Science Research Program through the National Research Foundation of Korea (NRF) funded by the Ministry of Education, Science and Technology under Contract No. 2012038593. Work of the MIT group is supported by the "Solid State Solar-Thermal Energy Conversion Center (S^3TEC), an Energy Frontier Research Center funded by the U.S. Department of Energy, Office of Science, Office of Basic Energy Sciences under Award Number: DE-SC0001299/DE-FG02-09ER46577 (Y.Y., D.K., G.C. for experiments and analysis), by AFOSR (G.C. for experimental system), and by DOE EERE Award No. DE-EE0005806 (D.K. and H.G. for heat recuperation analysis). We thank Dr. Bogyu Lim at Stanford University for measuring the heat capacity of CuHCF and we also thank Dr. Mauro Pasta at Stanford University for helpful discussion.

Author Contributions

S.W.L., Y.Y., G.C., and Y.C. conceived the idea, designed experiments, analyzed data, and wrote the paper. S.W.L., Y.Y, H.W.L., and H. G. carried out experiments. D.K. provide helpful suggestions and discussions. All the authors read the paper and made comments. G.C. and Y.C. directed the collaborative research.

Additional Information

The authors declare no competing financial interests. Supplementary Information accompany this paper online. Correspondence should be addressed to G.C. (gchen2@mit.edu) and Y.C. (yicui@stanford.edu).

Figure Legends

Figure 1 | Working principle of thermally regenerative electrochemical cycle (TREC) for thermal energy harvesting. a, Schematic view of thermal cycling: process 1, heating up the cell; process 2, charging at high temperature; process 3, cooling down the cell; process 4, discharging at low temperature. **b**, Temperature-entropy (T-S) diagram of thermal cycling assuming a temperature range between T_L and T_H. The theoretical energy gained over one cycle is the area of the loop determined by the temperature difference and entropy change.

Figure 2 | The electrochemical system for harvesting thermal energy with copper hexacyanoferrate (CuHCF) and Cu/Cu^{2+} electrodes. a, Voltage change of the CuHCF electrode, the Cu electrode, and the full cell compared to the initial voltage at 10 ℃ when the temperature varies from 10 to 70 ℃. The slopes of the fitting lines (gray) represent the temperature coefficients of electrodes and the full cell. **b**, Voltage plot of the cell during one cycle of thermal energy harvesting when the temperature is varied between 10 and 60 ℃ and the current density is 7.2 mA g^{-1}. The temperature of each process is shown by the gray dotted line, which is artificially superimposed for clarity. **c**, A voltage plot of the cell versus the specific charge capacity of CuHCF during one cycle with the same conditions as in (**b**). The red line represents heating (process 1) and charging (process 2) of the cell at 60 ℃, and the blue line represents cooling (process 3) and discharging (process 4) of the cell at 10 ℃.

Figure 3 | Efficiency of thermally regenerative electrochemical cycle (TREC). a, Efficiency of the cell cycle versus heat recuperation efficiency to be potentially included in the system when the temperature range is between 10 and 60 ℃ and the current density is 7.2 mA g^{-1}. Gray dotted

line represents the theoretical Carnot efficiency. **b**, Efficiency of the cell for various high temperatures (T_H) from 40 to 70 ℃ and two current densities, 7.2 and 17.9 mA g^{-1}, when the low temperature (T_L) is fixed at 10 ℃ and 50% heat recuperation efficiency is included in the calculation.

Figure 4 | Cycling performance of the thermally regenerative electrochemical system with copper hexacyanoferrate (CuHCF) and Cu/Cu^{2+} electrodes. a, Measured energy density and corresponding efficiency when 50% heat recuperation efficiency is included in the calculations. The cell is cycled between 20 and 50 ℃ and the current density is 17.9 mA g^{-1}. The asterisk denotes changing of the electrolyte because of drying after the 24th cycle. **b**, Voltage plot of the cell versus specific charge capacity of CuHCF during the 1st (dotted line) and 40th (solid line) cycles under the same conditions as in (**a**). The red and blue lines represent charging at 50 ℃ and discharging at 20 ℃, respectively.

Figure 1.

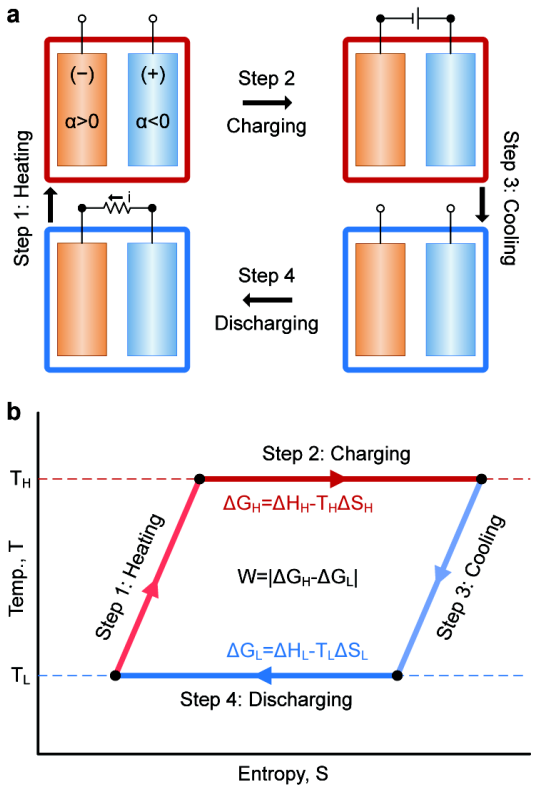

Figure 2.

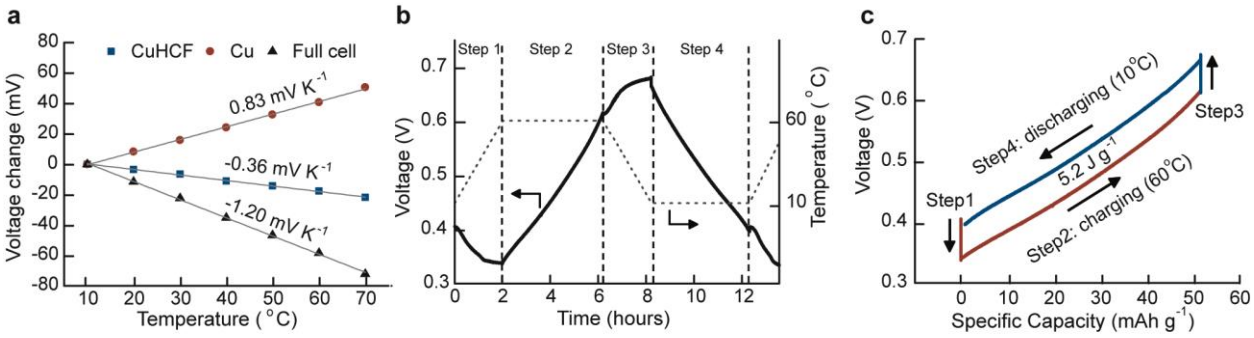

Figure 3.

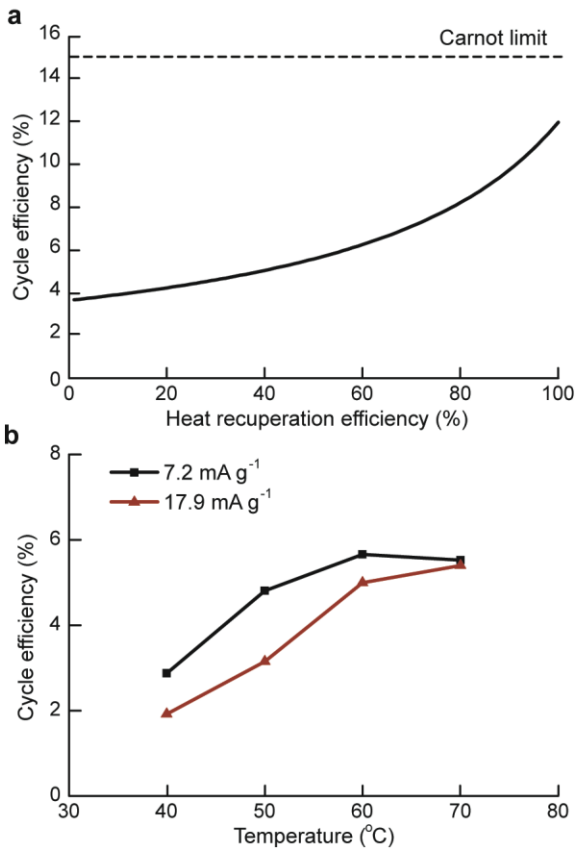
a
Carnot limit
Cycle efficiency (%)
Heat recuperation efficiency (%)
b
7.2 mA g-1
17.9 mA g-1
Cycle efficiency (%)
Temperature (°C)

Figure 4.

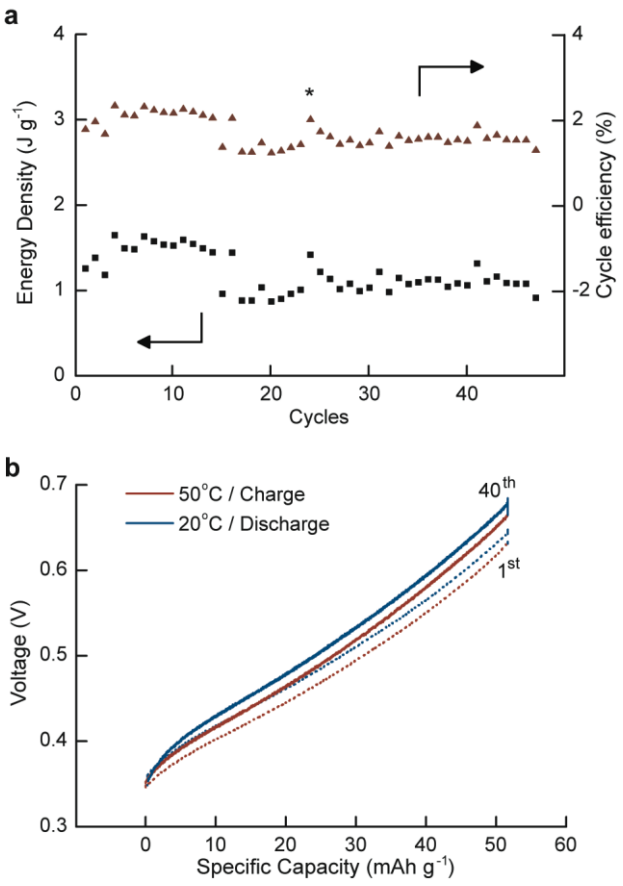
a
Energy Density (J g-1)
Cycle efficiency (%)
Cycles
*
b
50°C / Charge
20°C / Discharge
40th
1st
Voltage (V)
Specific Capacity (mAh g-1)

Supplementary Information

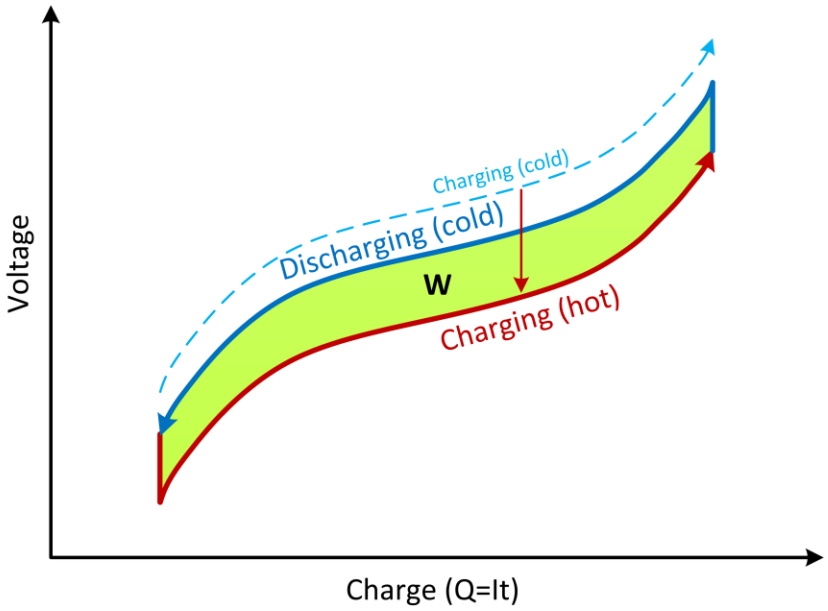

Supplementary Figure 1. Schematic voltage plot of the thermally regenerative electrochemical cycle (TREC) for thermal energy harvesting. Typical charging (dashed blue) and discharging (solid blue) voltage curves at the same temperature forms closed loop, the area of which means energy loss during a cycle. Negative temperature coefficient of the cell shifts down the charging curve at high temperature (solid red) below the voltage curve of discharging at low temperature (solid blue). The area of the closed loop between charging at the high temperature and discharging at the low temperature is the energy obtained during the cycle.

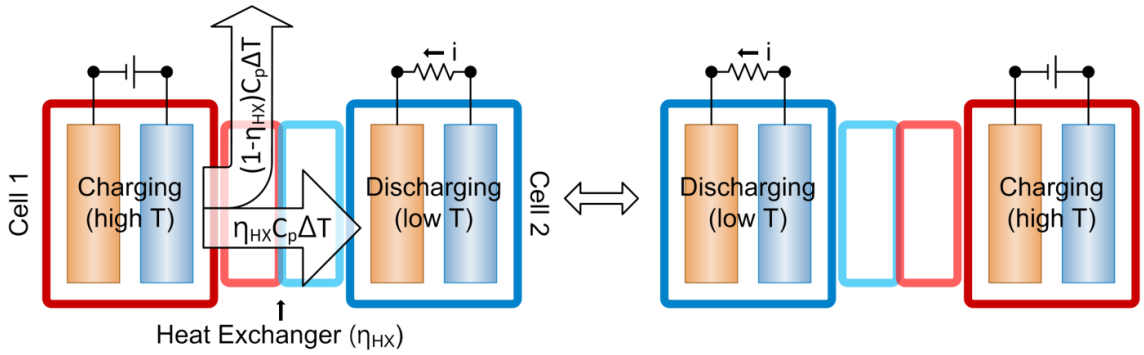

Supplementary Figure 2. Schematic view of energy flow at the heat recuperation during TREC. The energy stored in heat capacity of the hot cell is partially transferred to the cold cell; thus less energy is needed to heat up the cold cell.

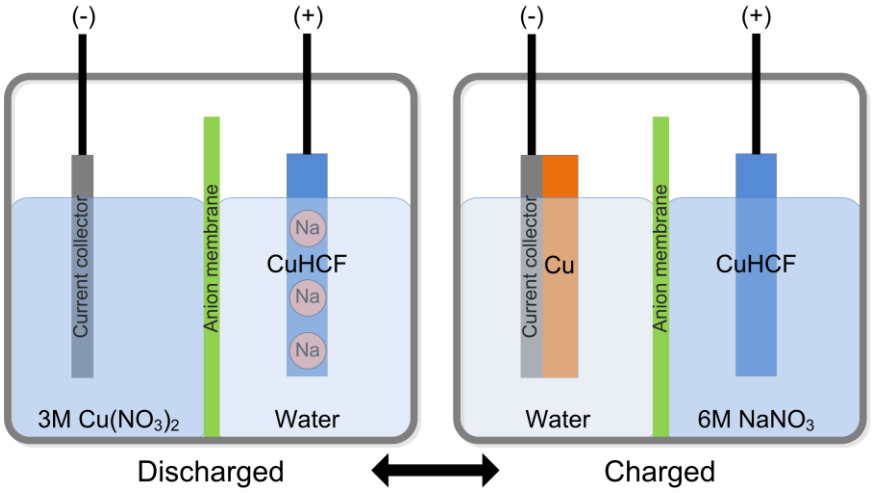

Supplementary Figure 3. Active materials in discharged and charged cell for consideration of heat capacity of the cell. The specific heat of the cell in discharged and charged states is calculated as the sum of all components.

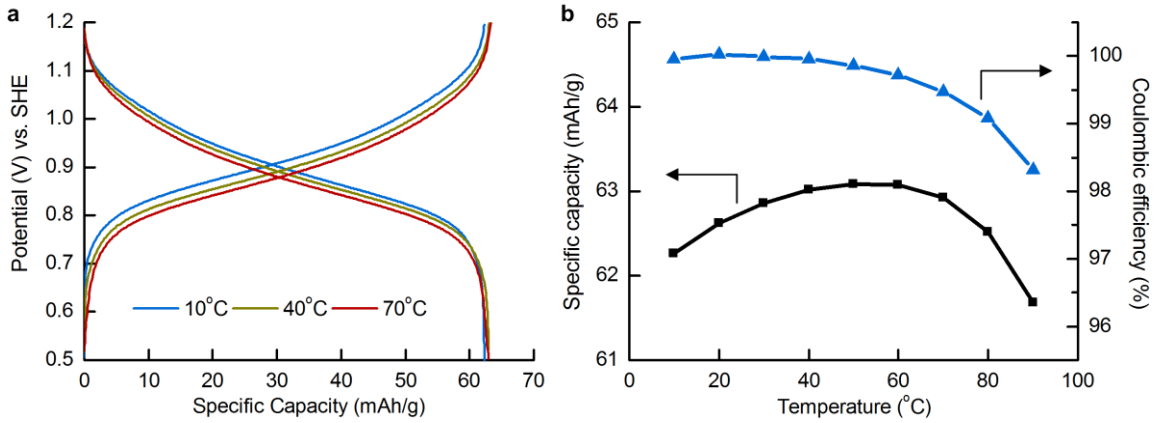

Supplementary Figure 4. Galvanostatic cycling test of half-cell of CuHCF at various temperatures from 10 to 90 ℃. a, Voltage for specific charge capacity of CuHCF half-cell with activated carbon counter electrode as a sodium ion sink at 10, 40, and 70 ℃. Cycling rate is 5C which takes about 24 min for charging and discharging. Typical curves of CuHCF are shown regardless temperature except shifting due to thermogalvanic effect. **b**, Average of specific charge capacity and Coulombic efficiency of 3 cycles at each temperature. Specific capacity increases as temperature is elevated but decreases significantly at above 60 ℃. Coulombic efficiency decreases slightly and its slope becomes stiffer upon increasing temperature.

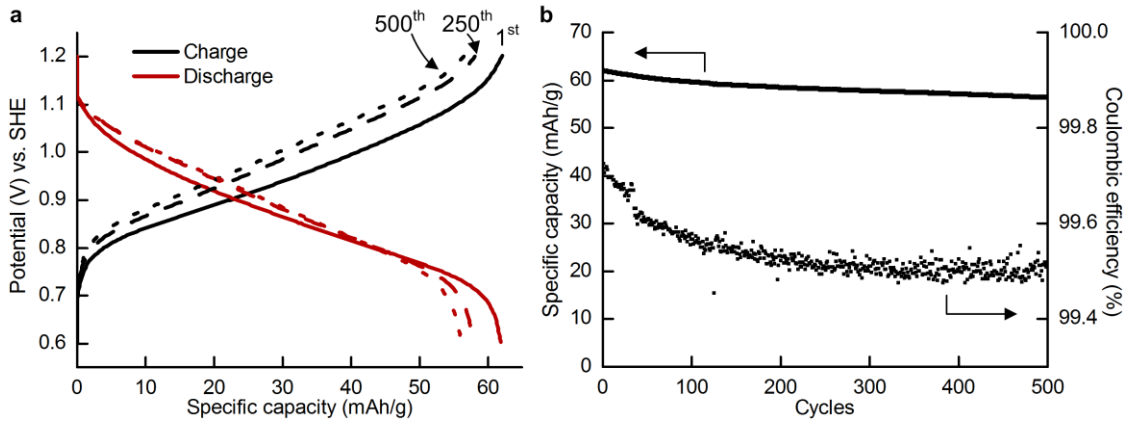

Supplementary Figure 5. Long term galvanostatic cycling of demonstrated electrochemical cell with 10C of cycling rate at 70 ℃. a, Voltage (vs. SHE) plot of CuCHF for its specific charge capacity. The curve doesn't change significantly after 250 and 500th cycles comparing with the curve of 1st cycle. But decaying of specific capacity is observed. **b**, Specific capacity and Coulombic efficiency for number of cycles. During 500 cycles, only 9.05% decaying of specific capacity was observed and Coulombic efficiency is saturated at 99.5%. The Coulombic efficiency in this test is higher than the result shown in Supplementary Fig. 6b at same temperature because of difference of cycling rate.

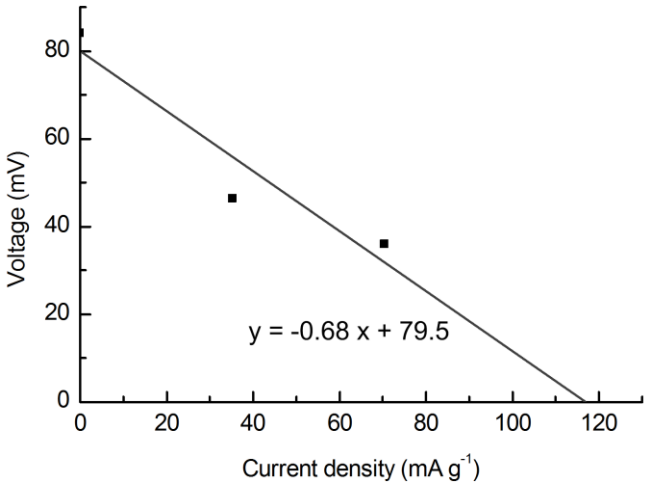

Supplementary Figure 6. Plot of voltage gap between charging and discharging voltage curve of TREC for various current densities when temperature is varied from 10 to 80 ℃. Gray solid line is linear fitting curve with assumption of linear relation of voltage gap and current density. The current density is based on the mass of all active materials and electrolytes.

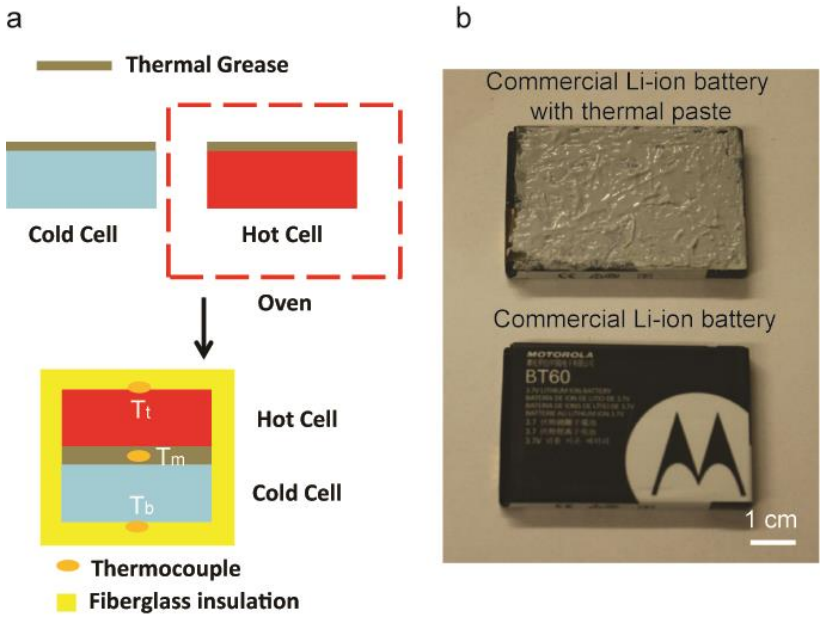

Supplementary Figure 7. Heat recuperation with a direct contact method. a, Scheme of heat recuperation by direct contact. Temperatures at the top of the hot cell (T_t), between two cells (T_m) and the bottom surface of the cold cell (T_b) are measured. **b**, Camera image of a commercial Li-ion battery with/without thermal paste. The weight of battery is 23.2 grams and paste is 0.7 grams.

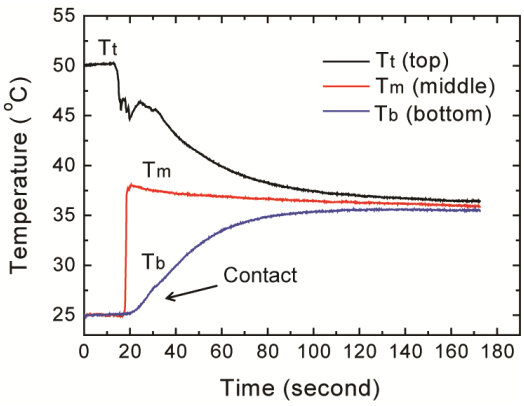

Supplementary Figure 8. Temperature change when a hot cell and a cold cell contact with each other. Hot cell quickly transfer heat to the cold cell.

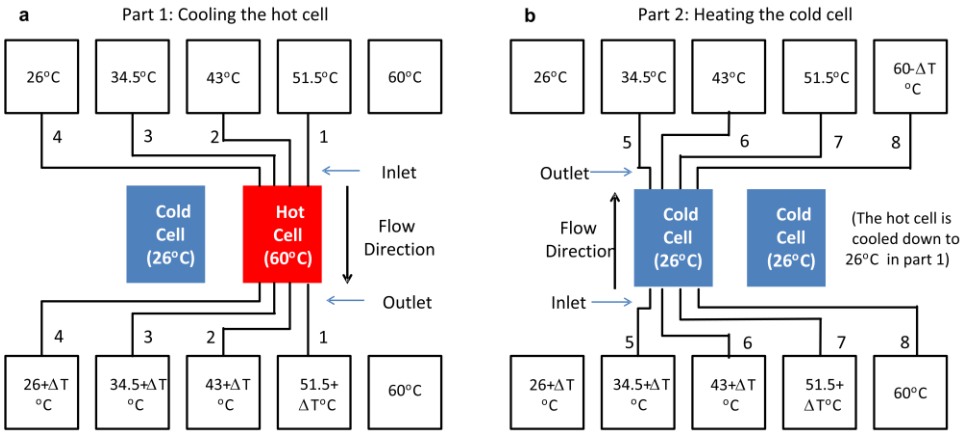

Supplementary Figure 9. Concept of step-wise cooling and heating of the hot and the cold cells to achieve high heat recuperation efficiency. The hot cell and the cold cell are initially at 26 and 60 ℃, respectively. **a**, The hot cell is cooled by reservoirs with HTFs at 51.5, 43, 34.5 and 26 ℃ (top) in sequence. **b**, The cold cell is heated with the slightly heated HTFs at 34.5, 43, 51.5 ℃ in sequence, recuperating the heat rejected from the hot cell. The last step in heating the cold cell from 51.5 °C to 60 ℃ uses an external heat source at 60 ℃. All reservoirs are connected to both cells with tubing, but those not in uses are not drawn in each part for simplicity.

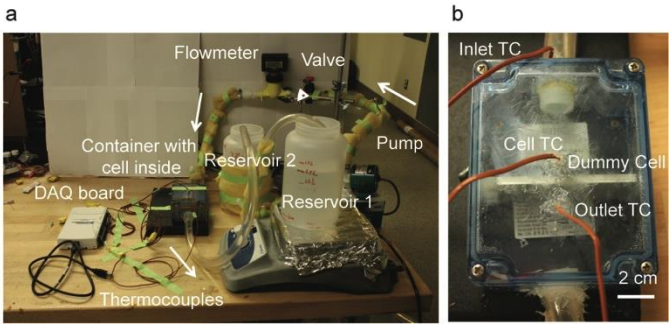

Supplementary Figure 10. Experimental Setup for step-wise heat recuperation experiments. a, Camera image of the heat exchange system. Water is pumped from reservoir 1 and its flow rate is controlled by valve and flowmeter. After exchanging heat with a stainless steel dummy cell in a plastic container, water drains to reservoir 2., A zoom-in image of the container with a dummy cell inside. K-type thermocouples are used to measure temperatures at inlet, cell and outlet.

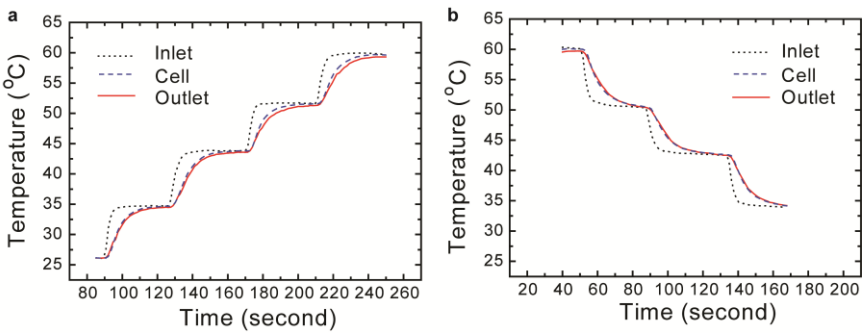

Supplementary Figure 11. Temperature changes in step-wise heat recuperation. The temperatures of inlet (T_{in}), outlet (T_{out}) and cell (T_{cell}) during the heating (**a**) and cooling (**b**) process. T_{out} and T_{cell} are very close to each other, indicating fast and efficient heat exchange. The gap between T_{in} and T_{out} indicates heat rejected from or lost to the cell.

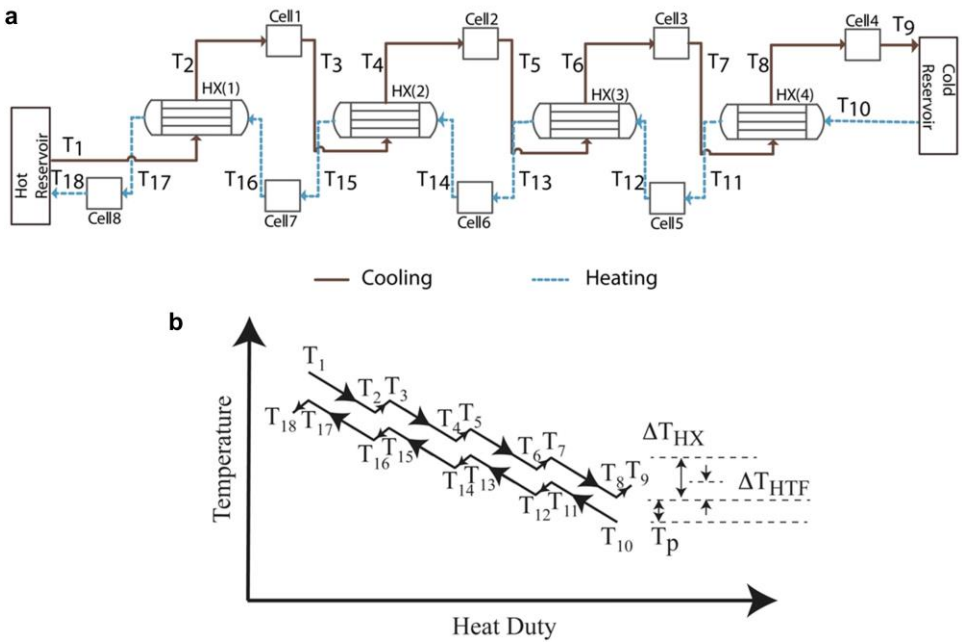

Supplementary Figure 12. Heat recuperation design with heat exchangers. a, A design for heat recuperation in TREC with heat exchangers. This design shows four heat recuperation steps, but it can be extended to any number of recuperation steps by adding more counter-flow HXs and cells. **b**, Pinch diagram of the considered $n = 4$ step heat recuperation cycle at a given time. T_1 and T_{10} are the temperatures of hot and cold reservoirs, respectively. Note that in an ideal case $T_p = 0$ and the two lines are in superposition of each other.

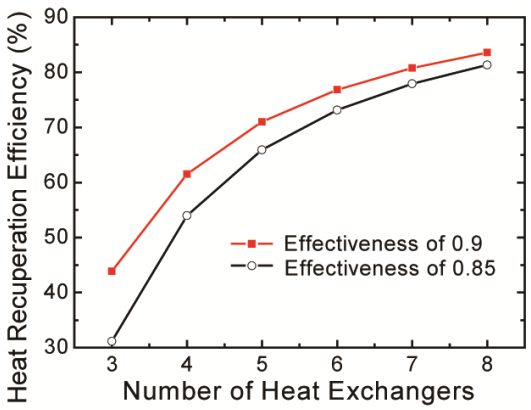

Supplementary Figure 13. Simulation on overall heat recuperation efficiency with different effectiveness of heat exchangers. The dependence of heat recuperation efficiency on the number of heat exchangers. The red and black line represent heat exchange effectiveness of 0.9 and 0.85, respectively.

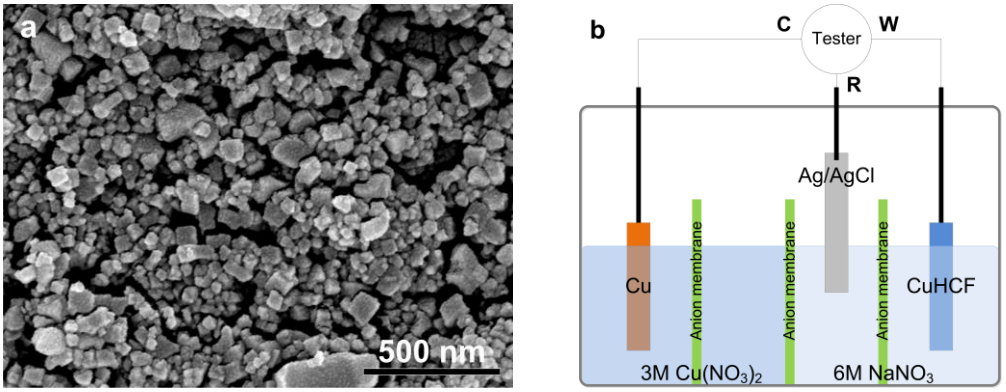

Supplementary Figure 14. Material synthesis and cell set up. **a**, SEM image of synthesized CuHCF. **b**, Schematic view of the demonstrated TREC cell.

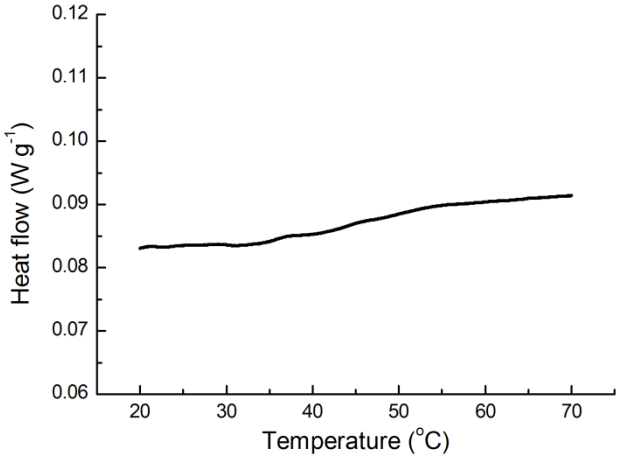

Supplementary Figure 15. The heat flux as a function of sample temperature in DSC tests of CuHCF. The specific heat (c_p) of the CuHCF was measured by Differential Scanning Calorimetry (DSC) test after drying the sample at 40~50 ℃ for more than 24 hours. The measurements were carried out by DSC Q100 (TA instrument). The measurement range was 20-70 ℃ with the ramping rate of 5 ℃/min. The heat flow curve is shown in Supplementary Fig. 5. The calculated c_p of CuHCF is 1.07 J $g^{-1}K^{-1}$.

Supplementary Tables

Supplementary Table 1. Parameters of electrode materials for calculation of Y

Electrode materials	α (mV K^{-1})	q_c (mAh g^{-1})	C_p (J K^{-1} g^{-1})	Y
CuHCF	-0.36	60	1.07	-0.073
CuHCF / 6M Na^+	-0.36	40.6	1.69	-0.031
Cu / 3M Cu^{2+}	0.83	117.4	2.80	0.125
	α (mV K^{-1})	q_c (mAh cm^{-3})	C_p (J K^{-1} cm^{-3})	Y
0.4 M $K_3Fe(CN)_6$ / $K_4Fe(CN)_6$	-1.4	22	4.18	0.027
Full cell CuHCF, electrolyte, Cu / 3M Cu^{2+}	-1.19	32.43 (mAh g^{-1})	2.048 (J K^{-1} g^{-1})	-0.068

Supplementary Table 2. Efficiency of previous thermocells and our TREC cell

	Electrolyte	T_H (^oC)	T_L (^oC)	Absolute Efficiency (%)	Note
Thermocell					
	Carbon/0.4 M $Fe(CN)_6^{3-/4-}$, 3 M K_2SO_4/Carbon	65	5	0.25	Ref [14]
	Cu/CuTAAB$(NO_3)_2$+ CuTAAB(NO_3) +KCl/Cu	95	20	0.34	Ref [12]
Our TREC					
	CuHCF/Cu^{2+}/Cu	60	10	3.7	No heat recuperation
	CuHCF/Cu^{2+}/Cu	60	10	5.7	50% heat recuperation
	CuHCF/Cu^{2+}/Cu	60	10	7.2	70% heat recuperation

Supplementary Table 3. The procedure for two steps in heating/cooling and heating/cooling time the same as charge/discharge time

Time Period	Cell No.					
	1	2	3	4	5	6
1	Cool 1	Cool 2	DC at T_L	Heat 1	Heat 2	C at T_H
2	Cool 2	DC at T_L	Heat 1	Heat 2	C at T_H	Cool 1
3	DC at T_L	Heat 1	Heat 2	C at T_H	Cool 1	Cool 2
4	Heat 1	Heat 2	C at T_H	Cool 1	Cool 2	DC at T_L
5	Heat 2	C at T_H	Cool 1	Cool 2	DC at T_L	Heat 1
6	C at T_H	Cool 1	Cool 2	DC at T_L	Heat 1	Heat 2
7 (same as 1)	Cool 1	Cool 2	DC at T_L	Heat 1	Heat 2	C at T_H

Supplementary Note:

Supplementary Note 1: Difference in temperature coefficients for isothermal cell and thermocell

The temperature coefficient of an electrochemical reaction can be defined experimentally in two ways, either as an "isothermal" or as a "thermal" temperature coefficient [24]. The isothermal temperature coefficient is defined when both electrodes are at the same temperature while the thermal temperature coefficient is when a temperature difference exists between the two electrodes. The isothermal coefficient $(dE/dT)_{iso}$ is the dependence of a redox reaction potential upon temperature in an isothermal cell, for example,

Negative electrode (−, T_1) /electrolyte (T_1) /positive electrode (+, T_1).

The reactions at the two electrodes are arbitrary. The isothermal coefficients for the electrode and full cell are defined as $a = \left(\frac{dE}{dT}\right)_{iso}$ and $a_c = \left(\frac{dV_{oc}}{dT}\right)_{iso}$, where E is the electrochemical potential of the electrode reaction and V_{oc} is the open circuit voltage of the full cell in isothermal condition. Obviously

$$\left(\frac{dV_{oc}}{dT}\right)_{iso} = \left(\frac{dE_+}{dT}\right)_{iso} - \left(\frac{dE_-}{dT}\right)_{iso}. \quad (1)$$

Or

$$a_c = a_+ - a_- \quad (2)$$

The subscript + and − indicates the positive and negative electrodes, respectively.

In contrast, thermal coefficient is the dependence of a redox reaction potential in a thermocell, or sometimes called thermogalvanic cell. The configuration of thermocell is similar to thermoelectric device:

M (T_1)/electrode (T_1)/ electrolyte / electrode (T_2)/M(T_2)

M is metal current collector. Thermal gradient exists in the electrolyte so that one end is at T_1 and the other end is at T_2. The same electrochemical reaction happens at both T_1 and T_2 but with opposite directions.

The difference between isothermal and thermal coefficient is quite small (<0.05 mV/K) as discussed below. In a TREC, what matters is the isothermal coefficient as the electrochemical cell is always under

isothermal condition. As a result, unless specified, all temperature coefficients (α) are the isothermal coefficients in this paper.

For a half electrode reaction A+ n e^- → B,

$$a_{A,B} = \left(\frac{dE}{dT}\right)_{iso} = \frac{s_B - s_A}{nF} = \frac{\Delta s}{nF} \tag{3}$$

where s_A and s_B are the partial molar entropy of A and B, respectively. *F* is the Faraday constant [24, 25].

For a full cell, if the spontaneous reaction in the isothermal cell can be written as Σ (Products – Reactants) = $\Sigma \nu_j B_j = 0$, where B_j is the *j* th chemical involved and ν_j is its stoichiometric number. Then

$$a_c = a_+ - a_- = \left(\frac{dV_{oc}}{dT}\right)_{iso} = \frac{\sum n_j s_j}{nF} \tag{4}$$

where s_j is the partial molar entropy of the *j* th chemical involved. *n* is the number of moles of electrons passed per ν_j mole of B_j reacted. *F* is the Faraday constant.

α_c can be either positive or negative, depending on the entropy change in the spontaneous direction. In order to convert heat to useful work, entropy change at T_H must be positive. In our CuHCF/Cu/Cu^{2+} system, α_c is negative and thus the process at high temperature (T_H) is charging so that entropy increases at T_H. In contrast, if α_c is positive, the process at T_H is discharging and the process at T_L is charging, so that entropy still increases at T_H.

The thermal coefficient needs to consider the entropy of ions and electrons transported from one electrode to the other as the two electrodes are at different temperatures [25]. For a simple reaction, A+n e^- → B

$$\left(\frac{dE}{dT}\right)_{th} = \frac{\Delta s - S_{ion}}{nF} - S_e \tag{5}$$

where $\Delta s = s_B - s_A$, the same as in an isothermal cell. S_{ion} is the entropy of ions transported in the electrolyte, or the so-called Eastman entropy[26, 27]. S_e is the Seebeck coefficient of metal. S_{ion}/nF is typically less than 0.05 mV K^{-1} unless the current is carried by H^+ and OH^- [24]. For KCl electrolyte, the value is ~ -0.02 mV K^{-1}, which is negligible [24]. S_e is also negligible for metals.

Compare equation 3 and 5, the difference between isothermal and thermal coefficient is

$$\left(\frac{dE}{dT}\right)_{iso} - \left(\frac{dE}{dT}\right)_{th} = \frac{S_{ion}}{nF} + S_e \tag{6}$$

which is less than 0.05 mV K^{-1} in general.

In our measurement, the thermal coefficient of Ag/AgCl/4 M KCl solution is measured first as the standard reference (0.12 ± 0.02 mV K^{-1}). Then it is converted to the isothermal coefficient by the assumption that $S_{ion}/nf + S_e = -0.02$ mV K^{-1}. Then the isothermal coefficients of electrode materials (CuHCF and Cu/Cu^{2+}) are measured against the Ag/AgCl/4 M KCl reference electrode in an isothermal cell. The uncertainty in the $S_{ion}/nF + S_e$ term leads to a small error (~0.02 mV K^{-1}) in the measured isothermal coefficient of an individual electrode. However, as shown below, it does not affect the coefficient of full cell, which determines the efficiency of the system. As Ag/AgCl is used as reference electrode, for the full cell, we have

$$\begin{aligned}\left(\frac{dE}{dT}\right)_{iso} &= \left(\frac{dE_+}{dT}\right)_{iso} - \left(\frac{dE_-}{dT}\right)_{iso} \\ &= \left[\left(\frac{dE_+}{dT}\right)_{iso} - \left(\frac{dE_{Ag/AgCl}}{dT}\right)_{iso}\right] - \left[\left(\frac{dE_-}{dT}\right)_{iso} - \left(\frac{dE_{Ag/AgCl}}{dT}\right)_{iso}\right]\end{aligned} \quad (7)$$

However, what we measure in experiment is the thermal (not isothermal) coefficient of Ag/AgCl, $\left(\frac{dE_{Ag/AgCl}}{dT}\right)_{th}$. So, apply equation 6 to 7, and then we have

$$\begin{aligned}\left(\frac{dE}{dT}\right)_{iso} &= \left[\left(\frac{dE_+}{dT}\right)_{iso} - \left(\frac{dE_{Ag/AgCl}}{dT}\right)_{iso}\right] - \left[\left(\frac{dE_-}{dT}\right)_{iso} - \left(\frac{dE_{Ag/AgCl}}{dT}\right)_{iso}\right] \\ &= \left[\left(\frac{dE_+}{dT}\right)_{iso} - \left(\frac{dE_{Ag/AgCl}}{dT}\right)_{th} - \frac{S_{ion}}{nF} - S_e\right] - \left[\left(\frac{dE_-}{dT}\right)_{iso} - \left(\frac{dE_{Ag/AgCl}}{dT}\right)_{th} - \frac{S_{ion}}{nF} - S_e\right] \\ &= \left(\frac{dE_+}{dT}\right)_{iso} - \left(\frac{dE_-}{dT}\right)_{iso}\end{aligned} \quad (8)$$

Consequently, the effect of $S_{ion}/nF+S_e$ term cancels each other in the full cell. This indicates that using thermal coefficient of Ag/AgCl reference electrode, $\left(\frac{dE_{Ag/AgCl}}{dT}\right)_{th}$, does not affect the accuracy of the isothermal coefficient of the full cell.

Supplementary Note 2: Design of heat recuperation for efficient heat harvesting

In order to enhance the efficiency of TREC, heat recuperation system can be employed to harvest heat rejected in the cooling process (process 3 in the main text) for heating in process 1 so that less external energy is needed in process 1. To realize this, a two-cell system is designed for efficient heat recuperation, as shown in Supplementary Fig. 2. The system contains two identical cells and one cycle contains the following four processes:

Process 1, heat is exchanged between cell 1 (T_H) and cell 2 (T_L). Some external energy is also needed as the heat recuperation efficiency is not 100%. At the end of process 1, cell 1 is at T_L and cell 2 is at T_H.

Process 2, cell 1 (T_L) is discharged and cell 2 (T_H) is charged.

Process 3, heat is exchanged again between cell 1 (T_L) and cell 2 (T_H). At the end of process 3, cell 1 is at T_H and cell 2 is at T_L.

Process 4, cell 1 (T_H) is charged and cell 2 (T_L) is discharged.

The operation of this two-cell system can be considered as independent cycle of each single cell with a time offset. Regarding to efficiency, all three terms in equation (2) (W, Q_H and Q_{HX}) in the manuscript doubles for the two-cell system compared to the cycle of a single cell, since processes of discharging, charging and heat exchanging all happen twice in one cycle now. As a result, the efficiency is the same as the single cell model in the main text and the single cell model is used to calculate the efficiency in this paper.

Supplementary Note 3: Theory on the efficiency of TREC

In this note, we are going to present the theory on the efficiency of TREC and derive equation (2) and (3) in the main text. Then in the next note we will present how to calculate the efficiency of TREC from our experimental results.

Let us consider a general condition: The reaction in the discharging process at T_L is Σ R $\rightarrow$ Σ P, *R* and *P* represents reactants and products, respectively. Then the high temperature process is the same reaction but in the opposite direction: Σ P $\rightarrow$ Σ R. In the following derivation, we are going to use subscript *dis* and *ch* to represent properties of Σ P and Σ R, respectively, as Σ P is in the discharged state and Σ R is in the charged state. For example, C_{dis} means the heat capacity of all materials in the discharged state (Σ P).

As discussed in the main text, the efficiency of a TREC is

$$\eta = \frac{\text{Net work output in one cycle}}{\text{Heat absorbed at } T_H + \text{External energy needed to heat the system up}} = \frac{W}{Q_H + Q_{HX}} \quad (9)$$

where W is the net work output in one cycle, Q_H is the heat absorbed at high temperature (T_H), Q_{HX} is the external energy needed to heat the system up.

W can be expressed as

$$W = W_{\max} - E_{loss} = -(\Delta G_H + \Delta G_L) - E_{loss} \quad (10)$$

where W_{max} is the maximum possible work in one cycle. ΔG is the change in Gibbs free energy in an electrochemical process (e.g. charge or discharge). E_{loss} is the energy loss due to internal resistance in electrochemical cells. The subscripts *H* and *L* represent the process at T_H and T_L, respectively and this applies to all thermodynamic functions in the following derivation. As ΔG = ΔH − TΔS, we have

$$\begin{aligned} W_{\max} &= -(\Delta H_H + \Delta H_L) + (T_H \Delta S_H + T_L \Delta S_L) \\ &= -(H_{ch,H} - H_{dis,H}) - (H_{dis,L} - H_{ch,L}) + (T_H S_{ch,H} - T_H S_{dis,H}) + (T_L S_{dis,L} - T_L S_{ch,L}) \\ &= (H_{ch,L} - H_{ch,H}) - (H_{dis,L} - H_{dis,H}) + (T_H S_{ch,H} - T_L S_{ch,L}) - (T_H S_{dis,H} - T_L S_{dis,L}) \end{aligned} \quad (11)$$

$$W_{\max} = -\int_{T_L}^{T_H} (C_{ch} - C_{dis})\,dT + \left[T_H S_{ch,H} - T_L \left(S_{ch,H} - \int_{T_L}^{T_H} \frac{C_{ch}}{T} dT \right) \right] - \left[T_H S_{dis,H} - T_L \left(S_{dis,H} - \int_{T_L}^{T_H} \frac{C_{dis}}{T} dT \right) \right] \quad (12)$$

In derivation above, $H_{ch,H}$ means the enthalpy of materials in the charged state at T_H, and other terms follow the same rule for explanation.

After rearrangement,

$$\begin{aligned} W_{\max} &= (T_H - T_L)(S_{ch,H} - S_{dis,H}) - \int_{T_L}^{T_H} (C_{ch} - C_{dis}) \left(1 - \frac{T_L}{T} \right) dT \\ &= \Delta T \Delta S_H - \int_{T_L}^{T_H} (C_{ch} - C_{dis}) \left(1 - \frac{T_L}{T} \right) dT \end{aligned} \quad (13)$$

where $\Delta T = T_H - T_L$, and $\Delta S_H = S_{ch,H} - S_{dis,H}$. Q_H can be expressed as

$$Q_H = T_H (S_{ch,H} - S_{dis,H}) = T_H \Delta S_H \quad (14)$$

For Q_{HX}, as a part of heat rejected in the cooling process can be used to heat the system up through a heat recuperation system, the external energy needed in the heating process is

$$Q_{HX} = C_{dis} \Delta T - \eta_{HX} C_{\min} \Delta T = \left[(1 - \eta_{HX}) C_{dis} + d\eta_{HX} (C_{dis} - C_{ch}) \right] \Delta T \quad (15)$$

$$d = \begin{cases} 1 & C_{dis} > C_{ch} \\ 0 & C_{dis} < C_{ch} \end{cases} \quad (16)$$

where C_{dis} is the total heat capacity of materials in the discharged state (the end of the discharge process at T_L), which needs to be heated. C_{ch} is the total heat capacity of materials in the charged state (the end of the charge process at T_H), which needs to be cooled down. C_{min} is the smaller one of C_{dis} and C_{ch}. All heat capacity and specific heat capacity in this paper is under constant pressure, so in general the subscript *p* is neglected. η_{HX} is the heat recuperation efficiency.

If the mismatch in heat capacity is negligible, $C_{ch} \approx C_{dis} = C_p$, then we have

$$h = \frac{DT\,DS_H - E_{loss}}{T_H DS_H + (1 - h_{HX})C_p DT} \quad (17)$$

which is equivalent to equation (2) in the main text.

To express the efficiency directly with material properties, we need to find out the relation between ΔS_H and measurable properties, such as temperature coefficient of the full cell (α_c). As shown above, the overall reaction in the full cell at T_H is Σ P $\rightarrow$ Σ R. This could be written as $\Sigma \nu_j B_j = 0$, where ν_j is positive for R and negative for P. Then

$$DS_H = \int_i^f \sum s_j dn_j \quad (18)$$

where s_j is the partial molar entropy of the *j* th chemical. n_j is the amount of *j* th chemical in the unit of mole. *i* and *f* represents the initial state (Σ P) and the final state (Σ R), respectively.

It is well known in physical chemistry that the extent of reaction (ζ), is equal for all chemicals involved in the reaction, as

$$z = \frac{n_j - n_{j0}}{n_j} \quad (19)$$

where n_{j0} is the amount of *j* th chemical at the initial state, and n_j is the amount of *j* th chemical at a certain time during the reaction. Then

$$DS_H = \int_i^f dz \sum n_j s_j \quad (20)$$

Equation 4 shows that the temperature coefficient of the full cell $a_c = \left(\frac{dV_{oc}}{dT}\right)_{iso} = a_+ - a_-$ is defined as $\frac{\sum n_j s_j}{nF}$ for the reaction in the spontaneous direction (discharge). In order to convert heat to useful work, ΔS_H must be positive at T_H. This means that the cell needs to be charged at T_H and discharged at T_L when α is negative, which is the case for the CuHCF//Cu^{2+}/Cu system. Then $\Delta S_H = \int_i^f a_c nF\, dz$. In contrast, when α is positive, the cell needs to be discharged at T_H and charged at T_L, and $\Delta S_H = -\int_i^f a_c nF\, dz$. Then we have

$$\Delta S_H = \begin{cases} \int_i^f a_c nF\, dz & a_c > 0 \\ -\int_i^f a_c nF\, dz & a_c < 0 \end{cases} \tag{21}$$

and it is always valid that

$$\Delta S_H = \int_i^f |a_c| nF dz \tag{22}$$

where n is the number of moles of electrons passed per ν_j mole of B_j reacted. F is the Faraday constant.

If we define the average temperature coefficient $\overline{a_c} = \oint a_c\, dz \Big/ \oint dz$, then

$$\Delta S_H = \left|\overline{\alpha_c}\right| nF \int_i^f d\zeta = \left|\overline{\alpha_c}\right| Q_{c\_ch}, \tag{23a}$$

$$Q_H = T_H \Delta S_H = \left|\overline{\alpha_c}\right| Q_{c\_ch} T_H \tag{23b}$$

where Q_{ch} is the total amount of charge transferred in the charging process at T_H.

Apply equation 23a to 17, we have

$$\eta = \frac{1 - E_{loss} \Big/ \left|\overline{\alpha_c}\right| Q_{c\_ch} \Delta T}{T_H / \Delta T + (1 - \eta_{HX}) C_p \Big/ \left|\overline{\alpha_c}\right| Q_{c\_ch}} \tag{24}$$

E_{loss} is the energy loss due to internal resistance of the cell. As W_{max} is the maximum energy difference between charge and discharge and W is the real difference in experiments, we have

$$W_{\max} = \oint I_{dis} V_{dis,eq}\, dt - \oint I_{ch} V_{ch,eq}\, dt \tag{25a}$$

$$W = \int I_{dis} V_{dis}\, dt - \int I_{ch} V_{ch}\, dt \tag{25b}$$

where the subscript *eq* indicates the corresponding open circuit voltage at a certain point in charge or discharge.

$$\begin{aligned} E_{loss} &= W_{\max} - W \\ &= \int I_{dis}(V_{dis,eq} - V_{dis})\, dt - \int I_{ch}(V_{ch,eq} - V_{ch})\, dt, \\ &= \int I_{dis}(I_{dis} R_{dis})\, dt - \int I_{ch}(I_{ch} R_{ch})\, dt \end{aligned} \tag{26}$$

where subscript *eq* indicates the open circuit voltage. R_{dis} and R_{ch} are the internal resistance at discharge and charge, respectively. The internal resistance term takes all effects into account, including electrode polarization and resistance of different components in the cell. In our experiments, $I_{dis} = I_{ch} = I$, If we assume that $Q_{c\_ch} = Q_{c\_dis} = Q_c$, R_{dis}, and R_{ch} are constants. Then we have

$$E_{loss} = Q_c I (R_{dis} + R_{ch}) \tag{27}$$

Obviously $R_{dis} + R_{ch} = R_L + R_H$, and

$$\eta = \frac{1 - I(R_H + R_L)/|\overline{\alpha_c}|\Delta T}{T_H/\Delta T + (1-\eta_{HX})C_p/|\overline{\alpha_c}|Q_c}. \tag{28}$$

Note that Carnot efficiency $\eta_c = \Delta T / T_H$. As α_c is nearly constant in the range of charge and discharge, we can apply the approximation that $\overline{\alpha_c} = \alpha$, the temperature coefficient at midpoint of the charging process, then

$$\eta = \frac{1 - I(R_H + R_L)/|\alpha|\Delta T}{1/\eta_c + (1-\eta_{HX})C_p/|\alpha|Q_c} = \eta_c \frac{1 - I(R_H + R_L)/|\alpha|\Delta T}{1 + \eta_c(1-\eta_{HX})/|Y|} \tag{29}$$

where $Y = \alpha Q_{c\_ch} / C_p$. The expression above is the same as equation (3) in the manuscript. If the system has a fast kinetics and thus low voltage hysteresis, $I(R_H + R_L)$ is negligible and the expression of efficiency is simplified to

$$h = h_c \frac{1}{1 + h_c(1 - h_{HX})/|Y|} \tag{30}$$

When only active materials in electrodes are considered,

$$Y = \frac{\alpha Q_{c\_ch}}{C_p} = \frac{(\alpha_+ - \alpha_-) m_+ q_{c,+}}{m_+ c_{p,+} + m_- c_{p,-}} \tag{31}$$

where q_c is the specific charge capacity and c_p is the specific heat. + and − represent positive and negative electrode, respectively. If the total charge capacities of two electrodes match each other,

$$m_+ q_{c,+} = m_- q_{c,-} \tag{32}$$

Then

$$Y = \frac{(\alpha_+ - \alpha_-)}{c_{p,+}/q_{c,+} + c_{p,-}/q_{c,-}} \tag{33}$$

If $\alpha_+ = -\alpha_- = \alpha$, $c_{p,+} = c_{p,-} = c_p$ and $q_{c,+} = q_{c,-} = q_c$, which means that the two electrodes have the same material properties but opposite signs of α,

$$Y = \frac{\alpha q_c}{c_p} \tag{34}$$

which can be defined as material figure of merit for TREC.

Supplementary Note 4: Calculation on the experimental efficiency of TREC

In this note, we are going to explain how experimental efficiency is calculated. Then the process to obtain equivalent ZT is illustrated. To calculate the experimental efficiency, we start with the general expression:

$$\eta = \frac{\text{Net work output in one cycle}}{\text{Heat absorbed at } T_H + \text{External energy needed to heat the system up}} = \frac{W}{Q_H + Q_{HX}} \tag{35}$$

Experimentally W is expressed as

$$W = \oint I_{dis} V_{dis}(t)\,dt - \oint I_{ch} V_{ch}(t)\,dt \tag{36}$$

which is the measured difference between discharge and charge energy. The subscripts *dis* and *ch* indicate discharge process and charge process, respectively. Consequently, the effect of non-100% Coulombic efficiency and voltage hysteresis are taken into account spontaneously as both I and V are experimental data. Q_H is calculated based on equation 23b:

$$Q_H = T_H \Delta S_H = \left|\overline{\alpha_c}\right| Q_{c\_ch} T_H = m_{CuHCF} q_{c\_ch} \left|\overline{\alpha_c}\right| T_H \tag{37}$$

where m_{CuHCF} and q_{ch} are the mass and specific charge capacity of CuHCF used in the charging process at T_H. As α_c shows a weak monotonously dependence on the extent of reaction ζ (< ±0.1 mV K^{-1}), it is a

good approximation to suppose $\overline{a_c} = a_c$ (50% state of charge), which is used in this paper to calculate Q_H. Regarding to Q_{HX}, according to equation 15

$$Q_{HX} = C_{dis}\Delta T - \eta_{HX} C_{\min}\Delta T = \left[(1-\eta_{HX})C_{dis} + \delta\eta_{HX}(C_{dis} - C_{ch})\right]\Delta T \tag{38a}$$

$$\delta = \begin{cases} 1 & C_{dis} > C_{ch} \\ 0 & C_{dis} < C_{ch} \end{cases} \tag{38b}$$

Therefore, the efficiency can be expressed as

$$\eta = \frac{\int I_{dis} V_{dis}(t)dt - \int I_{ch} V_{ch}(t)dt}{m_{CuHCF} q_{c\_ch} \alpha T_H + C_{dis}\Delta T - \eta_{HX} C_{\min}\Delta T} \tag{39}$$

If only active materials are considered in calculating Q_{HX}, and suppose that the amount of Na^+ and Cu^{2+} are just enough to provide charges needed for cycling. Then in charged state, the materials present in the system include: CuHCF (charged state), water on CuHCF side as all Na^+ intercalates into CuHCF and NO_3^- moves to the Cu side, 3 M $Cu(NO_3)_2$ as electrolyte on the copper side. In discharged state, the materials present in the system include: CuHCF (discharged state), 6 M $NaNO_3$ aqueous solution, water on Cu side as all Cu^{2+} is reduced to solid Copper, and solid copper as shown in Supplementary Fig. 3.

For better understanding of calculation of efficiency, detail of calculation with obtained numbers in our experiment is provided as an example. In our experiment when temperature is varied form 10 to 60 ℃ and current density is 7.2 mA g^{-1} as shown in Fig. 2C in main text, the net work output in one cycle is 17.700 mJ. The mass of CuHCF in charged state ($m_{CuHCF,ch}$) is 1.9828 mg, and the specific charge capacity (q_{c_CuHCF}) is 51.666 mAh/g. So the amount of charge needed for cycling is

$Q_{ch} = m_{CuHCF,ch} * q_{c\_CuHCF} = 0.3688$ C = 6 M * F * $V_{Elyte,\ Na^+}$ = 3 M * 2 * F * $V_{Elyte,Cu^{2+}}$

where $V_{Elyte,\ Na^+}$ and $V_{Elyte,\ Cu^{2+}}$ are the volume of 6 M $NaNO_3$ and 3 M $Cu(NO_3)_2$, respectively, F is the Faraday constant. Then,

$V_{Elyte,\ Na^+} = V_{Elyte,Cu^{2+}} = V_{Elyte} = 0.6371$ μL, and $m_{CuHCF,dis} = m_{CuHCF,ch}$ (1 + q_{c_CuHCF} / F * M_{Na} (22.99 g/mol) = 2.0707 mg

where $m_{CuHCF,dis}$ is the mass of CuHCF in discharged state.

Our measurements show that ρ_{Na^+} = 1.28 g/cm^3 and the water content in 6 M $NaNO_3$ is 60.2 wt%, and $\rho_{Cu^{2+}}$ = 1.37 g/cm^3 and the water content in 3 M $Cu(NO_3)_2$ is 58.8 wt%, where ρ_{Na^+} and $\rho_{Cu^{2+}}$ are the density of 6 M $NaNO_3$ and 3 M $Cu(NO_3)_2$.

Our experiments also show that

$c_{p\_CuHCF,ch}$ = 1.07 J/g K, $c_{p\_CuHCF,\,dis}$ = 1.066 J/g K ($c_{p\_CuHCF,\,dis}$ is estimated by Dulong-Petit law)

c_{p_Elyte,Na^+} = 2.998 J/g K, $c_{p\_Elyte,Cu^{2+}}$ = 2.80 J/g K

c_{p_Cu} = 0.385 J/g K, c_{p_water} = 4.18 J/g K

Then, at the discharged state, the total heat capacity of the system includes

CuHCF: $C_{p\_CuHCF,dis} = m_{CuHCF,dis} * c_{p\_CuHCF,dis}$ = 2.207 mJ/K

Water for Na^+ : $C_{p\_water,Na^+} = m_{Na^+} * 0.602 * c_{p\_water}$ = 2.052 mJ/K,

where C_{p_water,Na^+} is the heat capacity of water remained on the CuHCF side, and m_{Na^+} is the mass of 6 M $NaNO_3$ solution needed based on $V_{Elyte,\,Na^+}$ and ρ_{Na^+}.

3 M $Cu(NO_3)_2$: $C_{p\_Elyte,Cu2+} = m_{Cu2+} * c_{p\_Elyte,Cu2+}$ = 2.444 mJ/K

So the total heat capacity at the discharged state is

$$C_{p\_dis} = 6.703 \text{ mJ/K}$$

At the charged state, the total heat capacity of the system includes

CuHCF: $C_{p\_CuHCF,ch} = m_{CuHCF,ch} * c_{p\_CuHCF,ch}$ = 2.122 mJ/K

6 M $Na(NO_3)_2$ $C_{p\_Elyte,Na+} = m_{Na+} * c_{p\_Elyte,Na+}$ = 2.445 mJ/K

Water for Cu^{2+}: $C_{p\_water,Cu2+} = m_{Cu2+} * 0.588 * c_{p\_water}$ = 2.145 mJ/K,

where $C_{p\_water,Cu^{2+}}$ is the heat capacity of water remained on the CuHCF side, and $m_{Cu^{2+}}$ is the mass of 3 M $Cu(NO_3)_2$ solution needed based on $V_{Elyte,\,Cu^{2+}}$ and $\rho_{Cu^{2+}}$.

Solid Cu: $C_{p\_Cu} = m_{Cu} * c_{p\_Cu}$ = 0.0467 mJ/K

So the total heat capacity at the charged state is

$$C_{p\_ch} = 6.759 \text{ mJ/K}$$

For 50% heat recuperation efficiency, the amount of external energy needed is

$Q_{HX} / \Delta T = C_{p\_dis} - 0.5 * C_{p\_ch}$ = 3.323 mJ/K

ΔT =50 ℃. So,

$$Q_{HX}=166.171 \text{ mJ}.$$

The absorbed heat at T_H (Q_H) is calculated as

$$Q_H = |\alpha| * Q_{c\_ch} * T_H = 146.882 \text{ mJ}$$

And, net work output in one cycle in this experiment is measured as

$$W = 17.700 \text{ mJ}$$

Therefore, the efficiency of this case is calculated as 5.7 % and the equivalent ZT is 3.5 from the below equation.

For an ideal thermoelectric (TE) device, the relation between efficiency and ZT is:

$$h = \frac{DT}{T_H} \cdot \frac{\sqrt{1+ZT} - 1}{\sqrt{1+ZT} + T_c/T_H} \tag{40}$$

which can be written as

$$ZT = \left(\frac{DT + hT_L}{DT - hT_H} \right)^2 - 1 \tag{41}$$

To compare TREC with TE devices, we apply the efficiency of a TREC to equation 41 to obtain the equivalent ZT. This means that the thermoelectric device with the equivalent ZT working between the same hot and cold sources has the same efficiency as TREC. It is clear that the TREC efficiency included non-idealities such as the heat recuperation efficiency, and overvoltage potential, while the efficiency of TE expression is for an ideal device. However, it should be noticed that our calculations do not include components such as packaging and substrates.

Supplementary Note 5: Calculation of figure of merit (Y) of electrode materials

In supplementary note 3, $Y = \alpha\ q_c / c_p$, where q_c and c_p are the value per mass. However, for liquid electrode, it is more convenient to use the quantity per volume. Then

$$Y = \frac{aqr}{c_p r} = \frac{aq_{vol}}{c_{vol}} \tag{42}$$

where q_{vol} and c_{vol} are the charge capacity and heat capacity per volume.

The charge and heat capacity of CuHCF are calculated based on the mass of CuHCF and 6 M Na(NO_3) electrolyte needed to supply Na+ for reactions. The charge and heat capacity of Cu/Cu^{2+} are calculated

based on the mass of 3 M $Cu(NO_3)_2$ electrolyte, which is the oxidized state of Cu/Cu^{2+} electrode. The detail of the calculation of Y of electrodes is followed as below.

CuHCF / 6 M $NaNO_3$ electrolyte

Required volume of 6 M $NaNO_3$ electrolyte:

$V_{Elyte,\ Na^+}$ = Charge of CuHCF / (n * 6M * F) = m_{CuHCF} * q_{c_CuHCF} / (1 * 6 * 96485) = m_{CuHCF} * 0.06 *3600 [C g^{-1}] / (6 * 96485) [C L^{-1}] = 0.373 [cm^3 g^{-1}] * m_{CuHCF},

Where m_{CuHCF} is mass of CuHCF, q_{c_CuHCF} is specific charge capacity of only CuHCF (60 mAh g^{-1})

Specific charge capacity:

q_{c_CuHCF/Na^+} = charge of CuHCF / (mass of CuHCF + mass of 6M Na^+ electrolyte) = m_{CuHCF} * q_{c_CuHCF} / (m_{CuHCF} + ρ_{Na^+} * V_{Elyte,Na^+}) = m_{CuHCF} * q_{c_CuHCF} / (m_{CuHCF} + ρ_{Na^+} * 0.373 [cm^3 g^{-1}] * m_{CuHCF}) = 60 [mAh g^{-1}] / (1 + 1.28 * 0.373) = 40.6 mAh g^{-1},

where ρ_{Na^+} is the measured density of 6 M $Na(NO_3)$ electrolyte.

Specific heat:

c_{p_CuHCF/Na^+} = (heat capacity of CuHCF + heat capacity of 6M Na^+ electrolyte) / (mass of CuHCF + mass of 6M Na^+ electrolyte) = (m_{CuHCF} * c_{p_CuHCF} + ρ_{Na^+} * 0.373 [cm^3 g^{-1}] * m_{CuHCF} * c_{p_Elyte,Na^+}) / (m_{CuHCF} + ρ_{Na^+} * 0.373 [cm^3 g^{-1}] * m_{CuHCF}) = (c_{p_CuHCF} + ρ_{Na^+} * 0.373 [cm^3 g^{-1}] * c_{p_Elyte,Na^+}) / (1 + ρ_{Na^+} * 0.373 [cm^3 g^{-1}]) = (1.07 + 1.28 * 0.373*2.998) / (1 + 1.28 * 0.373) = 1.69 J g^{-1} K^{-1},

where c_{p_CuHCF} and c_{p_Elyte,Na^+} are specific heat of CuHCF and 6 M $Na(NO_3)$ electrolyte, respectively.

Figure of merit, Y

Y = $\alpha q_{c\_\ CuHCF/Na^+}$ / $c_{p\_\ CuHCF/Na^+}$ = -0.36*10^{-3} * 0.0406*3600 / 1.69 = -0.031

Cu / 3 M $Cu(NO_3)_2$ electrolyte

Specific charge capacity:

$q_{c\_Cu/Cu^{2+}}$ = charge of 3M Cu^{2+} electrolyte / mass of 3M Cu^{2+} electrolyte = (2 * 3M * F * $V_{Elyte,Cu^{2+}}$) / ($\rho_{Cu^{2+}}$ * $V_{Elyte,Cu^{2+}}$) = (2 * 3 * 96485) [C L^{-1}] / 1.37 [g cm^{-3}] = 422.6 C g^{-1} = 422.6 *1000 / 3600 = 117.4 mAh g^{-1},

where $V_{Elyte,Cu^{2+}}$ is volume of 3 M $Na(NO_3)_2$ electrolyte and $\rho_{Cu^{2+}}$ is density of 3 M $Na(NO_3)_2$ electrolyte.

Specific heat

$c_{p\_Elyte,Cu}^{2+}$ = 2.80 J g^{-1} K^{-1} (measured value)

Figure of merit, Y

$Y = \alpha q_{c\_Cu/Cu}^{2+} / c_{p\_Elyte,Cu}^{2+} = 0.83*10^{-3} * 0.1174*3600 / 2.80 = 0.125$

We can see that the high α of $K_3Fe(CN)_6/K_4Fe(CN)_6$ is compensated by the low charge capacity and high heat capacity. The low charge capacity is due to the the poor solubility of $K_3Fe(CN)_6/K_4Fe(CN)_6$ in water. The high heat capacity is a result of water solvent.

Y of demonstrated system is defined by difference of temperature coefficient of electrode materials, total specific charge capacity, and specific heat of the full cell. As shown in Supplementary Fig. 3, charged cell consists of charged CuHCF, 3M $NaNO_3$ electrolyte, water for Cu^{2+} ion, and Cu electrode. Then, detail of calculation of Y of the system is followed as below when 1g of mass of CuHCF is considered in the calculation ($m_{CuHCF,ch}$ = 1g).

At charged state, components of the full cell are Cu, water for Cu^{2+}, 6M $Na(NO_3)$, and charged CuHCF

Temperature coefficient:

$\alpha = |\alpha_{CuHCF} - \alpha_{Cu/Cu}^{2+}|$ = 1.19 mV K^{-1}

Specific charge capacity:

q_c = total charge / total mass = $q_{c\_CuHCF,ch} * m_{CuHCF,ch} / (m_{CuHCF,ch} + m_{Cu} + m_{water,Cu}^{2+} + m_{Elyte,Na}^{+}) = q_{c\_CuHCF,ch} * m_{CuHCF,ch} / (m_{CuHCF,ch} + q_{c\_CuHCF,ch} * m_{CuHCF,ch} / 2F * M_{Cu} + q_{c\_CuHCF,ch} * m_{CuHCF,ch} / (2F * 3M) * \rho_{Elyte,Cu}^{2+} *$ (water content) + $q_{c\_CuHCF,ch} * m_{CuHCF,ch} / (F * 6M) * \rho_{Elyte,Na}^{+}) = 60 *1 / (1 + 0.071 + 0.301 + 0.478) =$ 32.43 mAh g^{-1}

Specific heat:

Mass of each component is calculated above.

c_p = total heat capacity / total mass = $(c_{p\_CuHCF,ch} * m_{CuHCF,ch} + c_{p\_Cu} * m_{Cu} + c_{p\_water,Cu}^{2+} * m_{water,Cu}^{2+} + c_{p\_Elyte,Na}^{+} * m_{Elyte}) / (m_{CuHCF,ch} + m_{Cu} + m_{water,Cu}^{2+} + m_{Elyte,Na}^{+}) = (1.07 * 1 + 0.385 * 0.071 + 4.18 * 0.301 + 2.998 * 0.478) / (1 + 0.071 + 0.301 + 0.478) = 2.048$ J $K^{-1}g^{-1}$

$Y = \alpha q_c / c_p = 0.068$

Supplementary Note 6: Conceptual design and Experimental Validation of Heat Recuperation with High Efficiency

Heat recuperation is widely used in thermal systems. Commercial heat exchangers typically have effectiveness in the range of 70-90% [28]. Heat recuperation is also widely used in heat engines such as power plant and Stirling engines in different forms. Equation (3) in the manuscript shows that the efficiency of heat recuperation is crucial for the TREC system efficiency. Due to the low temperature differential between the hot and cold cells, and constant temperature operation at the charge and discharge states of the cycle we use, it is not apparent how to achieve highly efficient heat recuperation. Here, we first present a simple contact experiment showing a heat recuperation efficiency of 43.5%, followed by a design capable of achieving higher efficiency (60-70%), and test on key components to validate the design.

6.1 Direct Contact Heat Recuperation

One straightforward heat recuperation configuration is to directly contact the hot and the cold cell, which leads to a theoretical heat recuperation efficiency of 50%. We used commercial Motorola battery pack with a capacity of 1130 mAh and a mass of 23.2 grams. Its temperature is monitored by a thin thermocouple wires (130 μm) attached to its surface. The experimental process is illustrated in Supplementary Fig. 7. First both batteries are covered with the same amount of thermal paste (0.7 gram). One battery is placed in an oven set to 50 ℃ for 2 hours to equilibrate with the environment. The hot cell is subsequently removed from the oven and pressed onto the cold cell. The two cells are surrounded by fiberglass insulation during heat exchange. The temperature of the cold cell is calculated as the average of temperatures at the top (T_m) and bottom surfaces (T_b) of the cold cell.

The experimental results are shown in Supplementary Fig. 8. T_t, T_m and T_b are temperatures at the top of the hot cell, between two cells and at the bottom surface of the cold cell. The highest average temperature between T_m and T_b is 35.95 ℃ in the experiment. The temperature of the cold cell (T_C) and the hot cell (T_H) before contact are 25.0 and 50.2 ℃, respectively. Consequently, the heat recuperation efficiency is

$$(35.95\text{-}25.0)/(50.2\text{-}25.0)= 43.5\%$$

Such results indicate that heat recuperation efficiency of ~40% can be readily achieved in reality.

6.2 Step-Wise Heat Recuperation: Concept

The direct contact is limited to 50% recuperation efficiency. Higher efficiency can be achieved with more sophisticated design. We consider here the use of a liquid, such as water, as a heat carrier to transfer heat from hot TREC cells to cold TREC cells. Ideally, we would like to cool hot cells to the ambient temperature, and use energy rejected from hot cells to heat cold cells to the desired high operational temperature. A challenge is that temperature inversion happens: the original hot cells become cooler than the original cold cells, and cannot transfer heat rejected from the originally hot cell to the originally cold cell after this temperature inversion.

To overcome this challenge, we develop a step-wise process. In this scheme, hot cells are cooled by multiple thermal reservoirs from high to low temperature in sequence, then the reservoirs transfer absorbed energy to cold cells step by step from low temperature to high temperature. This ensures that the heat transfer between hot cells and cold cells happen at a small temperature difference with high effectiveness.

The design of such system is illustrated in Supplementary Fig. 9. Suppose that initially the hot cell is at 60 ℃ and the cold cell is at 26 ^{o}C (room temperature). The reservoir at 26 ℃ is the ambient, and the reservoir at 60 ℃ is the external heat source. We cool down the hot cell and heat up the cold cell step by step using intermediate hot and cold reservoirs containing a heat transfer fluid (HTF, water for example) at different temperatures (51.5 ℃, 43 ℃, 34.5 ℃ in the illustrated example). Here, we use reservoirs to explain the step-wise heat recuperation concept. These hot and cold reservoirs will be replaced by heat exchangers in practical systems as explained in supplementary note 6.4. The cooling of the hot cell originally at 60 ℃ will be done by four steps using HTF at 51.5, 43, 34.5 and 26 ℃, respectively. In each step, the HTF temperature increases slightly, absorbing heat from the hot cell. The heated HTFs at 34.5, 43 and 51.5 ℃ are diverted to cold cells in sequence (Supplementary Fig. 9b) to transfer the gained heat to the cold cell. If the effectiveness of heat exchange between the cell and HTFs is 1 (as we will demonstrate experimentally next), there is no energy loss for reservoirs at 34.5, 43 and 51.5 ℃, since all heat received from the hot cell is transferred to the cold cell. The only extra energy needed is the last step in heating, warming the cold cell to 60 ℃ using an external reservoir at 60 ℃, which is C_c*8.5 K with C_c the heat capacity of the cell in the unit of J K^{-1}. Consequently the heat recuperation efficiency (η_{HX}) is

$$1 - C_c*8.5\ K / C_c*(60\ ℃ - 26\ ℃) = 75\%$$

In general, if there is n+1 reservoirs at T_L, $T_L+\Delta T$, $T_L+2\Delta T$,….. and T_H ($\Delta T= (T_H-T_L)/n$),

$$h_{HX} = \frac{n - 1}{n} \tag{43}$$

6.3 Experimental Validation of the Step-wise Heat Recuperation System

To validate the step-wise heat recuperation approach, we build a prototype system as shown in Supplementary Fig. 10. For each heat exchange step, water is pumped from reservoir 1 (1.5 L) with a flow rate of 2.3 liter per minute. The pumped water flows through a chamber with a dummy battery inside and drains to the other empty reservoir (reservoir 2). After each step of heat exchange, reservoir 1 and 2 are replaced by another set of reservoirs at a different temperature for the next step. Water flown to reservoir 2 in the heating process is used in the cooling process. We use a dummy cell made of 304 stainless steel, which has a thermal diffusivity (4×10^{-6} m^2 s^{-1}) similar to batteries (10^{-6} to 10^{-5} m^2 s^{-1}) [29]. The size of the dummy battery is 3.3 cm × 7 cm × 0.6 cm. In comparison, a typical phone battery has size of 3 cm × 5 cm × 0.5 cm (Motorola) To calculate the heat exchanged between water and the cell, temperatures at the inlet, cell and outlet are measured with K-type thermocouples (TCs) and recorded with a DAQ board at a frequency of 10 Hz. The cell temperature is measured with a thermocouple embedded in a hole drilled in the center of the cell (Supplementary Fig. 10b).

Supplementary Fig. 11 shows the measured temperature at the inlet (T_{in}), cell (T_{cell}) and outlet (T_{out}) during heating and cooling. In the experiment, heating (part 2 in Supplementary Fig. 9) is performed before cooling (part 1 in Supplementary Fig. 9). This switch does not change any results on efficiency, as cells in real system go through cyclic process, as explained in supplementary note 6.5. T_{in} behaves like a step function as the temperature of reservoirs changes from 26 ℃ to 60 ℃ and decreases back to 34.5 ℃ step by step. The last step in cooling (34.5 -> 26 ℃) is not performed as heat harvested in this step cannot be used for heating in following cycles and thus it is not used in any calculations. T_{cell} and T_{out} gradually respond to T_{in} due to the heat capacity of the dummy cell. The highest T_{cell} and T_{out} reached are 59.6 ℃ at the end of heating. The fast and efficient heat exchange between cell and water is reflected by the small difference between T_{cell} and T_{out}. The negligible temperature difference justifies the assumption of effectiveness of 1 for the heat exchange between the cell and the HTF.

Based on equation 43, the theoretical efficiency of the procedure above is (4-1)/4 = 75%. The experimental heat recuperation efficiency is expressed as

$$h_{ex} = \frac{\text{Heat rejected from the hot cell to reservoirs at 51.5, 43, and 34.5 °C}}{\text{Heat absorbed by the cold cell from reservoirs at 34.5, 43, 51.5, and 60 °C}} \quad (44)$$

In the i th step, heat rejected to the reservoir (Q_i) is

$$Q_i = \int \dot{m} C_{water} \Delta T \, dt \tag{45}$$

where $\dot{m}$ is the volumetric flow rate of water in the unit of $m^3 s^{-1}$, C_{water} is the heat capacity of water in the unit of J m^{-3} K^{-1}. $\Delta T = T_{out}-T_{in}$. Q_i is positive for the cooling process and negative for the heating process.

In experiments, the flow rate $\dot{m}$ is kept constant by the flowmeter and valve. C_{water} is nearly a constant between 26 and 60 ℃ (~0.1% difference). Thus, based on Supplementary Fig. 11 and equation 44 and 45, we have

$$h_{ex} = - \frac{\sum \text{cooling with reservoirs at 51.5, 43, and 34.5 °C} \int \Delta T \, dt}{\sum \text{heating with reservoirs at 34.5, 43, 51.5, and 60 °C} \int \Delta T \, dt} = - \frac{-225.5Ks}{329.5Ks} = 0.684 \tag{46}$$

The achieved experimental efficiency (68.4%) is close to the theoretical value (75%). The difference is likely a result of heat loss through walls of the container. More detailed analysis shows that the heat dissipation loss becomes negligible (~1%) when the system dimension increases to about one meter, suggesting that the experimental efficiency could reach ~74%. In addition, by further increasing the number of reservoirs, we believe that the heat recuperation efficiency can be even over 80%.

6.4 Step-wise Design with Heat Exchangers Instead of Thermal Reservoirs

The design and experiments above clearly demonstrate that heat recuperation efficiency of 70% is reasonable. In reality, thermal reservoirs at different temperatures can be made through mixing hot water and water at ambient temperature with different ratios. This method does not result in any energy loss. However, it is more practical and compact to use heat exchangers to create HTFs at different temperatures for heat exchange with TREC cells. In the following part, we analyze the heat recuperation efficiency of a system with heat exchangers instead of thermal reservoirs at intermediate temperatures. Although the overall efficiency becomes lower as extra loss exists due to effectiveness of heat exchangers, the analysis shows that the design is capable of achieving efficiency of 60-70%.

The system structure is presented in Supplementary Fig. 12. This figure shows the case with eight TREC cells and four heat exchangers (HXs, n = 4), while real systems can use more cells and HXs to increase efficiency. In this design, two HTF streams are utilized to transport thermal energy from hot cells to cold cells. Each cell in this configuration undergoes a transient heat transfer with the HTF.

In this design, each cell is cooled/heated by multiple steps with HTFs at the outlet of HXs, which acts as thermal reservoirs in supplementary note 6.2. Cell 1-4 are in the cooling process and Cell 5-8 are in the

heating process. Two reservoirs, one at high temperature (T_1) and one at ambient temperature (T_{10}), are utilized to assist the heat transfer process.

Starting from left to right, HTF with the temperature of T_1 is introduced in HX1 and its temperature at the outlet is reduced by ΔT_{HX} (e.g. T_1-T_2). The HTF exchanges heat with Cell 1 and its temperature is increased by ΔT_{HTF} (e.g. T_3-T_2) to recuperate some of the thermal energy of Cell 1. Subsequently, the HTF flows through other HXs and cells in sequence going through the same heat transfer processes at lower temperatures before exiting the recuperation step at temperature of T_9. On the other side, the HTF with the inlet temperature T_{10} is introduced in HX4, absorbs thermal energy and then flows through cell (5) transferring some of its thermal energy to the cell. The temperature of HTF drops by ΔT_{HTF} in this process. Then, it flows through other HXs and cells in sequence undergoing the same heat transfer processes at higher temperatures. The corresponding pinch diagram is shown in Fig. 12b. At the end of this step, temperatures of cells become the same as that of HTFs. Temperatures of cell 1-4 are at T_3, T_5, T_7 and T_9 while the temperatures of cell 5-8 are at T_{12}, T_{14}, T_{16} and T_{18}. In this way, heat exchange happens between cells with small temperature difference (e.g. cell 3 and 5) and thus higher recuperation efficiency is realized. After this step, cells are disconnected from that stream and connected to another HX for the next recuperation step. Connection and disconnection are realized by automatic valves in the practical system.

This heat recuperation method can be further developed to a practical continuous procedure that contains all four steps (discharge, heating, charge and cooling) in the cycle, which will be explained later in supplementary note 6.5 continuous operation.

According to the manuscript, the heat recuperation efficiency is defined as

$$h_{HX} = \frac{\text{Heat absorbed by the n cold cells - Energy extracted from the hot reservoir}}{\text{Heat rejected in cooling the n hot cells}} \quad (47)$$

As heat recuperation is a cyclic process, we only need to consider energy change in a certain step.
Assuming all cells and the temperature difference between cells are identical, the efficiency is written as

$$h_{HX} = \frac{n\int MC_{cell}\,dT_{cell} - \int \dot{m}C_{HTF}(T_1 - T_{18})dt}{n\int \dot{m}C_{HTF}\Delta T_{HTF}dt} \quad (48)$$

where T_{18} is the temperature of THF flowing into the hot reservoir. M is the mass of a cell and C_{cell} is the specific heat of a cell (J Kg^{-1} K^{-1}). T_{cell} is the temperature of a cell. $\dot{m}$ is the flow rate of HTF in the unit of

kg s^{-1}. C_{HTF} is the specific heat of the HTF (J Kg^{-1} K^{-1}). ΔT_{HTF} is the temperature difference of HTF before and after heat exchange with the cell. The integral is from the beginning to the end of one step. If the effectiveness of heat exchange between cells and HTFs is 1, which is close to what we demonstrated, we have

$$\int MC_{cell}\, dT_{cell} = \int \dot{m} C_{HTF} \Delta T_{HTF}\, dt \tag{49}$$

From Supplementary Fig. 12b,

$$T_1 - T_{18} = T_p + \Delta T_{HTF} \tag{50}$$

Suppose that $\dot{m}$ and C_{cell} are constant during heat recuperation. Apply equation 49 and 50 to 48, we have

$$h_{HX} = \frac{\int \left[(n-1)\Delta T_{HTF} - T_p \right] dt}{\int n \Delta T_{HTF}\, dt} = \frac{(n-1)\overline{\Delta T_{HTF}} - \overline{T_p}}{n\overline{\Delta T_{HTF}}} \tag{51}$$

where $\overline{\Delta T_{HTF}}$ and $\overline{T_p}$ are the time-averaged value of corresponding integrals. This equation illustrates that the system efficiency is $h_{HX} = \frac{n-1}{n}$ with ideal HXs (T_p = 0), which converges to the configuration with thermal reservoirs in supplementary note 6.2, since HTFs at outlets of HXs act as thermal reservoirs and there is no loss within HXs.

As the effectiveness of a heat exchanger is defined as

$$e = \frac{\dot{q}}{\dot{q}_{\max}} = \frac{\Delta T_{HX}}{\Delta T_{HX} + T_p} \approx \frac{\Delta T_{HX}}{\Delta T_{HX} + \overline{T_p}} \tag{52}$$

Thus, the pinch temperature difference can be expressed in terms of the effectiveness and replaced in the recuperation efficiency,

$$h_{HX} = \frac{(n-1)\overline{\Delta T_{HTF}} - \Delta T_{HX}\left(\frac{1-e}{e}\right)}{n\overline{\Delta T_{HTF}}} \tag{53}$$

If we define $\Delta T = T_1 - T_{10} = T_p + n\Delta T_{HX} - (n-1)\overline{\Delta T_{HTF}}$, which is the temperature difference between the hot and the cold source. Then

$$\Delta T_{HX} = \frac{\left(\frac{\Delta T}{n}\right) + \frac{n-1}{n}\overline{\Delta T_{HTF}}}{1 + \frac{1-\varepsilon}{n\varepsilon}} \tag{54}$$

Thus, η_{HX} is only a function of the given parameters ΔT, n, ε, and $\overline{\Delta T_{HTF}}$. Note that the effectiveness of heat exchange between the HTF and the cell is assumed 1 as demonstrated experimentally in the previous note.

The dependence of η_{HX} on the number of heat exchangers is plotted in Supplementary Fig. 13 at two different heat exchanger effectiveness that are available for commercial heat exchangers [28]. This figure shows that over 50% heat recuperation efficiency can be readily achieved with *n* larger or equal to 4 and 80% heat recuperation efficiency is achievable.

6.5 Continuous Operation

To realize a continuous process with heat exchangers, all cells in the system are divided into four groups: discharge at T_L, heating, charge at T_H and cooling. At each moment, certain amount of cells is operated in each group, and each cell undergoes all four groups in a whole cycle. For example, Supplementary Table 3 shows the procedure for a system with two-step heating/cooling and that charge/discharge time is the same as cooling/heating. In this procedure, each cell operates through the four steps with a time offset so that the whole process is continuous. Cool 1 represents the cooling process from T_H to $(T_H+T_L)/2$ and Cool 2 is from $(T_H+T_L)/2$ to T_L. Heat 1 is from T_L to $(T_H+T_L)/2$, and Heat 2 is from $(T_H+T_L)/2$ to T_H. C and DC represent for charge and discharge, respectively. For each cell, the switch between different cooling steps and heating steps is realized by opening and closing valves between cells and heat exchangers.

In general, if the step number for heating/cooling is *n*, and the ratio of discharge/charge time to cooling/heating time of each step is *m*, then *n* cells are in heating and cooling, respectively while *m* cells are in discharge and charge, respectively.

Supplementary Note 7: Power density of TREC

For a two-cell system described in Supplementary note 2, the general expression of the power rate per cell is

$$P = \frac{(V_{dis} - V_{ch})I}{2} \tag{55}$$

The factor 2 counts for the fact that two identical cell exists in the system. This expression is the same for a single cell configuration (Fig. 1a). Time for heat recuperation is neglected as it is short compared to charge/discharge time. Subscripts *dis* and *ch* are for discharge and charge, respectively.

From supplementary note 3 and 4, we know that

$$V = V_{eq} - IR \tag{56}$$

V_{eq} is the open circuit voltage of the cell. R is the internal resistance of the cell and it takes both electrode polarization and resistance of different components into account.

When current is not large, R could be considered as a constant. This is valid based on our experiments (see part below) and previous literature on thermogalvanic cells [14]. Then

$$P = \frac{(V_{dis,eq} - IR_{dis} - V_{ch} - IR_{ch})I}{2} \tag{57}$$

As $V_{dis,eq} - V_{ch,eq} = \alpha\Delta T$

$$P = \frac{a\Delta T - I(R_{dis} + R_{ch})I}{2} I \tag{58}$$

Obviously

$$P_{\max} = \frac{(a\Delta T)^2}{8(R_{dis} + R_{ch})}, \text{ when } I = \frac{a\Delta T}{2(R_{dis} + R_{ch})}. \tag{59}$$

Under the condition of P_{max},

$$h_{p_{\max}} = \frac{1}{2} h(I = 0) = \frac{1}{2} h_{\max} \tag{60}$$

Experimentally, we could plot the average voltage gap between charging and discharging ($\alpha\Delta T - I (R_{dis} + R_{ch})$) against current rate (I). Then $R_{dis} + R_{ch}$ is extracted as the slope of linear fitting curve, and P_{max} can be calculated.

In order to demonstrate power density capability of TREC in this study, energy harvesting is tested at wider temperature range and simplified cell configuration with one membrane although its cycle efficiency becomes lower due to decreasing Coulombic efficiency. The difference of charging and discharging voltage at same state of charge and current density are considered for estimation of power

density. But for heating and cooling time of the cell in the cycle is not counted in the estimation. Supplementary Fig. 6 shows the plot of average voltage gap between charging and discharging voltage curves for various current densities of TREC cycled between 10 and 80 ℃. When the current density is zero, the voltage gap (V_g) is the change of open-circuit voltage (84 mV) due to temperature change. The voltage gap decreases to 46.4 and 35.9 mV when the current density increases to 35.3 and 70.4 mA g^{-1}, respectively. (The mass of active materials, including CuHCF, electrolyte for Na^+, copper, and water for Cu^{2+} are considered for calculation of current density and power density.) Short circuit current (I_{sc}) is calculated as 116.9 mA g^{-1}. Consequently, the maximum power is 1.2 mW g^{-1} when the current density is 58.5 mA g^{-1}. Equivalent C-rate of the above current density for maximum power density is 1.7C which means that a cycle of charging and discharging takes 1 hour when used specific capacity in the cycle is 50 mAh g^{-1} for mass of CuHCF, 83% of its typical specific capacity. In the experiments for temperature range from 10 to 60 ℃ as shown in Fig. 3b in the manuscript, OCV is 66 mV and the voltage gap decreases to 59 and 36.3 mV when the current densities are 7.2 and 17.9 mA g^{-1}, respectively. The short circuit current is fitted as 40 mA g^{-1} and current density for the maximum power density is 20 mA g^{-1}. In the experiment, the applied current density of 17.9 mA g^{-1} is close to the value for achieving maximum power density, and the efficiency is as high as 5.0 % with an equivalent ZT of 2.7.

References

1. Chu, S. & Majumdar, A. Opportunities and challenges for a sustainable energy future. *Nature* **488**, 294-303 (2012).
2. Rattner, A.S. & Garimella, S. Energy harvesting, reuse and upgrade to reduce primary energy usage in the USA. *Energy* **36**, 6172-6183 (2011).
3. Rosi, F.D. Thermoelectricity and thermoelectric power generation. *Solid-State Electronics* **11**, 833-868 (1968).
4. DiSalvo, F.J. Thermoelectric cooling and power generation. *Science* **285**, 703-706 (1999).
5. Bell, L.E. Cooling, heating, generating power, and recovering waste heat with thermoelectric systems. *Science* **321**, 1457-1461 (2008).
6. Poudel, B. et al. High-thermoelectric performance of nanostructured bismuth antimony telluride bulk alloys. *Science* **320**, 634-638 (2008).
7. Paradiso, J.A. & Starner, T. Energy Scavenging for Mobile and Wireless Electronics. *IEEE Pervasive Computing* **4**, 18-27 (2005).
8. Kraemer, D. et al. High-performance flat-panel solar thermoelectric generators with high thermal concentration. *Nature materials* **10**, 532-538 (2011).
9. Snyder, G.J. & Toberer, E.S. Complex thermoelectric materials. *Nature materials* **7**, 105-114 (2008).

10. Zebarjadi, M., Esfarjani, K., Dresselhaus, M.S., Ren, Z.F. & Chen, G. Perspectives on thermoelectrics: from fundamentals to device applications. *Energy & Environmental Science* **5**, 5147-5162 (2012).
11. Zhao, L.D. et al. Ultralow thermal conductivity and high thermoelectric figure of merit in SnSe crystals. *Nature* **508**, 373-377 (2014).
12. Kuzminskii, Y.V., Zasukha, V.A. & Kuzminskaya, G.Y. Thermoelectric effects in electrochemical systems. Nonconventional thermogalvanic cells *Journal of Power Sources* **52**, 231-242 (1994).
13. Quickenden, T.I. & Mua, Y. A review of power generation in aqueous thermogalvanic cells. *Journal of The Electrochemical Society* **142**, 3985-3994 (1995).
14. Hu, R. et al. Harvesting waste thermal energy using a carbon-nanotube-based thermo-electrochemical cell. *Nano letters* **10**, 838-846 (2010).
15. Gunawan, A. et al. Liquid Thermoelectrics: Review of Recent And Limited New Data of Thermogalvanic Cell Experiments. *Nanoscale and Microscale Thermophysical Engineering* **17**, 304-323 (2013).
16. Hesson, J.C. & Shimotake, H. in Regenerative EMF Cells, Vol. 64. (eds. C.E. Crouthamel & H.L. Recht) 82-104 (American Chemical Society, Washington, D.C.; 1967).
17. Chum, H.L. & Osteryoung, R.A. Review on thermally regenerative electrochemical system. (1981).
18. Hammond, R.H. & William M. Risen, J. An electrochemical heat engine for direct solar energy conversion. *Solar Energy* **23**, 443-449 (1979).
19. Wessells, C.D., Huggins, R.A. & Cui, Y. Copper hexacyanoferrate battery electrodes with long cycle life and high power. *Nature communications* **2**, 550-554 (2011).
20. Pasta, M., Wessells, C.D., Huggins, R.A. & Cui, Y. A high-rate and long cycle life aqueous electrolyte battery for grid-scale energy storage. *Nature communications* **3**, 1149-1155 (2012).
21. Wessells, C.D., Peddada, S.V., McDowell, M.T., Huggins, R.A. & Cui, Y. The effect of insertion species on nanostructured open framework hexacyanoferrate battery electrodes. *Journal of The Electrochemical Society* **159**, A98-A103 (2012).
22. Bejan, A. & Kraus, A.D. Heat Transfer Handbook. (Wiley-Interscience, 2003).
23. Serth, R.W. Process heat transfer: Principles and applications. (Academic Press, New York; 2007).
24. deBethune, A.J., Licht, T.S. & Swendeman, N. The temperature coefficients of electrode potentials : The Isothermal and Thermal Coefficients --The Standard Ionic Entropy of Electrochemical Transport of the Hydrogen Ion. *Journal of The Electrochemical Society* **106**, 616-625 (1959).
25. Anderson, L.B., Greenberg, S.A. & Adams, G.B., Vol. 64 213-276 (1967).
26. Eastman, E.D. Electromotive force of electrolytic thermocouples and thermocells and the entropy of transfer and absolute entropy of ions. *Journal of american chemical society* **50**, 292-297 (1928).
27. Agar, J.N., Mou, C.Y. & Lin, J.-l. Single-Ion Heat of Transport in Electrolyte Solutions. A Hydrodynamic Theory. *J. phys. Chem.* **93**, 2079-2082 (1989).
28. Adrian Bejan , A.D.K. Heat Transfer Handbook. (Wiley-Interscience, 2003).
29. Hossein Maleki, S.A.H., J. Robert Selman, Ralph B. Dinwiddie, H. Wang Thermal Properties of Lithium-Ion Battery and Components. *Journal of The Electrochemical Society* **146**, 947-954 (1999).